NeuroImage 65 (2013) 34–51

Contents lists available at SciVerse ScienceDirect

NeuroImage

journal homepage: www.elsevier.com/locate/ynimg

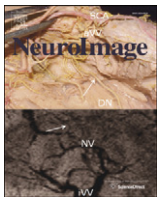

The emergence of abnormal hypersynchronization in the anatomical structural network of human brain

Boyuan Yan *, Peng Li

Department of Electrical and Computer Engineering, Texas A&M University, College Station, TX 77843, USA

ARTICLE INFO

Article history:
Accepted 12 September 2012
Available online 19 September 2012

Keywords:
Global synchronization
Brain structural connectivity
Spike-wave discharges

ABSTRACT

Brain activity depends on transient interactions between segregated neuronal populations. While synchronization between distributed neuronal clusters reflects the dynamics of cooperative patterns, the emergence of abnormal cortical hypersynchronization is typically associated with spike-wave discharges, which are characterized by a sudden appearance of synchronous around 3 Hz large amplitude spike-wave discharges of the electroencephalogram. While most existing studies focus on the cellular and synaptic mechanisms, the aim of this article is to study the role of structural connectivity in the origin of the large-scale synchronization of the brain. Simulating oscillatory dynamics on a human brain network, we find the space–time structure of the coupling defined by the anatomical connectivity and the time delays can be the primary component contributing to the emergence of global synchronization. Our results suggest that abnormal white fiber connections may facilitate the generation of spike-wave discharges. Furthermore, while neural populations can exhibit oscillations in a wide range of frequency bands, we show that large-scale synchronization of the brain only occurs at low frequencies. This may provide a potential explanation for the low characteristic frequencies of spike-wave discharges. Finally, we find the global synchronization has a clear anterior origin involving discrete areas of the frontal lobe. These observations are in agreement with existing brain recordings and in favor of the hypothesis that initiation of spike-wave discharges originates from specific brain areas. Further graph theory analysis indicates that the original areas are highly ranked across measures of centrality. These results underline the crucial role of structural connectivity in the generation of spike-wave discharges.

Introduction

Normal brain function requires the dynamic interaction of functionally specialized but widely distributed cortical regions. Long-range synchronization of oscillatory signals has been suggested to mediate these interactions within large-scale cortical networks by dynamically establishing task-dependent networks of cortical regions (Varela et al., 2001). Disturbances of such synchronized networks have been implicated in several brain disorders, such as schizophrenia, autism, epilepsy, Alzheimer's disease, and Parkinson's disease (Uhlhaas and Singer, 2006). Especially, while synchronization between distributed neuronal clusters reflects the dynamics of cooperative patterns, the emergence of abnormal cortical hypersynchronization is typically associated with the occurrence of ~3 Hz spike-wave discharges (SWD) recorded on the electroencephalogram (EEG). The sudden appearance of SW patterns from a normal background leads to the traditional concept of sudden hypersynchronous and widespread activity during generalized seizures.

The mechanisms underlying spike-wave patterns are complex and may involve cerebral cortex and thalamus, intrinsic properties of neurons, and various types of synaptic receptors present in the circuit. There has been notable effort devoted to understanding seizure dynamics and various hypotheses have been proposed to explain the underlying mechanisms (Lytton, 2008; Yan and Li, 2011). Some studies (Destexhe, 1998; Destexhe et al., 1996, 1998; Giaretta et al., 1987; Pollen, 1964) demonstrate that synaptic receptors are especially important in the generation of epileptic seizures while others believe intrinsic properties of neurons play an important role (de Curtis et al., 1998; Dichter and Ayala, 1987; Halliwell, 1986; Schwindt et al., 1988; Timofeev and Steriade, 2004; Timofeev et al., 2004; Wong and Prince, 1978). While those studies shed light on the intrinsic and synaptic mechanisms of seizure generation, they do not take into consideration the structural connectivity, which may play an important role in the emergence of global synchronization.

Traditionally, the abnormality of structural connectivity is often explored in a localized pathologic brain region, which is typically the focus of partial seizures. For example, in (Dyhrfjeld-Johnsen et al., 2007; Santhakumar et al., 2005), the abnormal structural changes (mossy fiber sprouting, mossy cell death, etc) in dentate gyrus are studied to explore the genesis of temporal lobe epilepsy. Recently, the role of structural connectivity underlying generalized epilepsies has received more and more attention. From computational perspectives, in (Benjamin et al., 2012), a phenomenological model of seizure initiation is used to demonstrate that network structure (identified from EEG) in patients with idiopathic generalized epilepsies correlates with smaller

* Corresponding author.
E-mail addresses: byan@tamu.edu (B. Yan), pli@tamu.edu (P. Li).

1053-8119/$ – see front matter © 2012 Elsevier Inc. All rights reserved.
http://dx.doi.org/10.1016/j.neuroimage.2012.09.031

escape times relative to network structures from controls, suggesting that network structure may play an important role in seizure initiation and seizure frequency. Using the same model, the study in (Terry et al., 2012) demonstrates that EEG discharge representing either generalized or focal seizure arises purely as a consequence of subtle changes in network structure, without the requirement for any localized pathological brain region. In (Goodfellow et al., 2011), the authors show that in an extended local area of cortex, spatial heterogeneities in a model parameter can lead to spontaneous reversible transitions from a desynchronized background to synchronous SWD due to intermittency.

While successfully demonstrating the potential role of network structure underlying generalized epilepsies, none of these studies has been done based on the time-space structure of biologically realistic connectivity of human brain. In fact, as explicit time delays are neglected, these studies are restricted to interacting local populations. To explain the emergence of synchronization at large spatial scales ranging up to almost 20 cm, we believe the network structure of the brain should be taken into consideration. The anatomical connections between areas of the brain form a structure network upon which various neural activities unfold. Brain areas are dynamically coupled to one another forming functional networks associated with perception, cognition, and action, as well as during spontaneous activity in the default or resting state. Existing computational studies demonstrate the important role of the characteristic "small-world" structure of the underlying connectivity matrix between different brain areas in the spontaneous emergence of spatio-temporally structured network activities (Cabral et al., 2011; Deco et al., 2009, 2011; Ghosh et al., 2008; Honey et al., 2007, 2009). Especially, recent studies (Cabral et al., 2011; Deco et al., 2009) have revealed that resting state activity (the temporally coherent activity in the absence of an explicit task) is closely related to the underlying anatomical connectivity. During rest, spontaneous blood oxygen level dependent (BOLD) signal is characterized by slow fluctuations (<0.1 Hz) and anti-correlated spatiotemporal patterns. By modeling each brain region as a neural oscillator and simulating in a biologically realistic brain network, the slow fluctuating and anti-correlated spatiotemporal patterns have been linked to fluctuations in the neural activity and synchrony in the gamma range. Especially, the most agreement of the simulated results with the empirically measured results has been found for a set of parameters (coupling, delay, noise, etc) where subsets of brain areas tend to synchronize in clusters while the network is not globally synchronized.

The aim of this article is to study the role of structural connectivity in the mechanistic origin of the large-scale synchronization of the brain, which may relate to the spread of SW epileptic seizure activity. While synchronization phenomenon in large populations of interacting elements has been widely studied in many areas of natural science, mathematics, and social science (Arenas et al., 2008), there has been little work done specifically considering the space–time structure of a biologically realistic cortical network. To reveal the role of brain structural connectivity in the emergence of such global synchronization, we perform a simulation study based on biologically realistic connectivity of brain areas. The structural connectivity was derived from a macroscopic cortico-cortical connectivity network derived from a diffusion-magnetic resonance imaging (MRI) data set using the method in (Zalesky and Fornito, 2009). The connectivity between all brain area pairs is quantified by a connectivity strength matrix and a fiber length matrix. Different from exiting works (Cabral et al., 2011; Deco et al., 2009, 2011; Ghosh et al., 2008; Honey et al., 2007, 2009), in which the neural dynamics at each brain area is modeled by a single neural oscillator (FitzHugh–Nagumo oscillator, Wilson–Cowan oscillator, etc), we use a system of coupled phase oscillators described by Kuramoto (1984) models to represent neural dynamics at each local brain area. Therefore, the proposed model is capable of representing not only the synchronization on a global level but also the local synchronization on different brain areas.

Specifically, to take into consideration the interplay of local and global processes at different time scales, we use local coupling strength, global coupling strength, time delay, and intrinsic frequency as independent parameters. An extensive exploration of the parameter space illustrates that the space–time structure of the coupling defined by the anatomical connectivity and the time delays can be the primary component contributing to the emergence of global synchronization. Our results will show that the global synchronization is highly dependent on the time delays and the intrinsic frequencies of the oscillators. To highlight the crucial role of interrelationship between local processes and the global activity, we further characterize the initialization of synchronization in both time and space. Our results will demonstrate that the initialization of global synchronization has a clear anterior origin involving discrete areas of the frontal lobe. While experimental observations of frontal epileptic focus do exist (Amor et al., 2009; Holmes et al., 2004; Pavone and Niedermeyer, 2000), there is a lack of understanding of the underlying mechanism. In this paper, by performing graph theory analysis of the structural connectivity, we will point out that the initialized areas of global synchronization ("hot spots") correspond to the nodes with highest degree of centrality ("structural hubs"). This once again underscores the crucial role of structural connectivity in the generation of SW epileptic seizures.

Methods

Structural connectivity

We use the structural connectivity between 80 cortical areas of the human brain. The areas are divided according to a functional subdivision of the cortex derived from the automated anatomical labeling (AAL) atlas (Tzourio-Mazoyer et al., 2002). The structural data for brain connectivity is provided by Andrew Zalesky and Alex Fornito. The structural connectivity is obtained from a macroscopic cortico-cortical connectivity network derived from a diffusion-magnetic resonance imaging (MRI) data set using the algorithm proposed in (Zalesky and Fornito, 2009).

In (Zalesky and Fornito, 2009), a new DTI-derived measure of cortico-cortical connectivity is established based on the notion of information flow. The measure is intended to reflect the maximum rate at which information can be transmitted between a pair of cortical regions, which is quantified by the net capacity of all interconnecting fiber bundles. The set of all voxels comprising DTI space is first partitioned into two sets: white-matter $\mathcal{W}$, and grey-matter $\mathcal{G}$ using either manual tracing or any of a number of automated segmentation algorithms. The set $\mathcal{G}$ is then subdivided into N continuous cortical regions according to existing functional subdivision of interest to the researcher. Then, a 3-D lattice scaffolding for white-matter is constructed by drawing a link between each pair of voxels in a 26-voxel neighborhood for which their two respective principal eigenvectors form a sufficiently small angle. Let g_i be the set of voxels comprising cortical region $i=1,\ldots,N$. Let $E(i)\in\mathcal{W}$ denote the set of white-matter voxels comprising the interface cortical region g_i. A path between a pair of nodes u and v is said to be an (i,j)-*path* if $u\in E(i)$ and $v\in E(j)$. Let $f_{i,j}$ denote the maximum number of link-disjoint $(i,j)-$paths that can be established. Since the capacity of a fiber bundle is measured as the maximum number of link-disjoint paths that can be established between opposing ends of a fiber bundle, the net capacity provided by all fiber bundles interconnecting cortical region g_i and g_j, given by $f_{i,j}$, is used as a measure of connectivity strength.

The connectivity between all brain area pairs is quantified by two 80×80 matrices: a connectivity strength matrix $\mathbf{C}$ and a fiber length matrix $\mathbf{L}$. As described above, the connectivity strength is estimated based on the density of the white fiber tracts, which is given by the net capacity of fiber bundles $f_{i,j}$. The length of fiber connecting two brain areas is calculated as the average length across all the fibers connecting them. Both matrices are obtained by averaging over 31

control subjects. Since tractography does not give fiber directionality, both matrices are symmetric.

The human brain is divided into two hemispheres (left and right). There are 40 different anatomical areas in each hemisphere. As each area appears in both hemispheres, the total number is 80. For the same anatomical area in different hemispheres, there are different indices and labels. The list of 40 anatomical areas is given in Fig. 1(C). For each area, it shows the index and label in the right hemisphere (RH), the index and label in the left hemisphere (LH), the name of the area, and the corresponding anatomical region it belongs to. The connectivity strength matrix **C** and fiber length matrix **L** are shown in Figs. 1(A) and (B), respectively. The connectivity strength is normalized so that the maximal strength is 1 ($max(\mathbf{C}_{pq}) = 1$, $p, q = 1, \ldots, P$), where P is the total number of areas and $P = 80$ for the current model. The intra-area

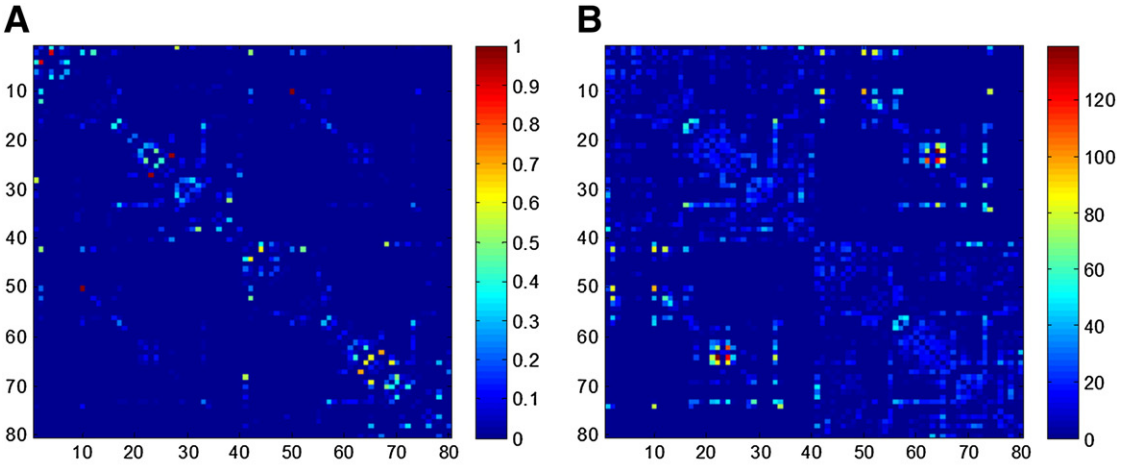

C

List of cortical areas

Index (RH)	Label (RH)	Index (LH)	Label (LH)	Coritcal area name	Anatomical regions
1	PRE_R	41	PRE_L	Precentral gyrus	Central region
2	F1_R	42	F1_L	Super frontal gyrus, dorsolateral	Frontal lobe
3	F1O_R	43	F1O_L	Super frontal gyrus, orbital part	Frontal lobe
4	F2_R	44	F2_L	Middle frontal gyrus	Frontal lobe
5	F2O_R	45	F2O_L	Middle frontal gyrus, orbital part	Frontal lobe
6	F3OP_R	46	F3OP_L	Inferior frontal grus, opercular part	Frontal lobe
7	F3T_R	47	F3T_L	Inferior frontal grus, triangular part	Frontal lobe
8	F3O_R	48	F3O_L	Inferior frontal gyrus, orbital part	Frontal lobe
9	RO_R	49	RO_L	Rolandic operculum	Frontal lobe
10	SMA_R	50	SMA_L	Supplementary motor area	Frontal lobe
11	OC_R	51	OC_L	Olfactory cortex	Frontal lobe
12	F1M_R	52	F1M_L	Supeiror frontal gyurs, medial	Frontal lobe
13	F1MO_R	53	F1MO_L	Supeiror frontal gyurs, medial orbital	Frontal lobe
14	GR_R	54	GR_L	Gyrus rectus	Frontal lobe
15	IN_R	55	IN_L	Insula	Insula
16	ACIN_R	56	ACIN_L	Anterior cingulate and paracingulate gyri	Limbic bole
17	MCIN_R	57	MCIN_L	Median cingulate and paracingulate gyri	Limbic bole
18	PCIN_R	58	PCIN_L	Posterior cingulate gyrus	Limbic bole
19	HIP_R	59	HIP_L	Hippocampus	Limbic bole
20	PHIP_R	60	PHIP_L	Parahippocampal gyrus	Limbic bole
21	V1_R	61	V1_L	Calcarine fissure and surrounding cortex	Occipital lobe
22	Q_R	62	Q_L	Cuneus	Occipital lobe
23	LING_R	63	LING_L	Lingual gyrus	Occipital lobe
24	O1_R	64	O1_L	Superior occipital gyrus	Occipital lobe
25	O2_R	65	O2_L	Middle occipital gyrus	Occipital lobe
26	O3_R	66	O3_L	Inferior occipital gyrus	Occipital lobe
27	FUSI_R	67	FUSI_L	Fusiform gyrus	Occipital lobe
28	POST_R	68	POST_L	Postcentral gyrus	Central region
29	P1_R	69	P1_L	Superior parietal gyrus	Parietal lobe
30	P2_R	70	P2_L	inferior parietal, but supramarginal and angular gyri	Parietal lobe
31	SMG_R	71	SMG_L	Supramarginal gyrus	Parietal lobe
32	AGr_R	72	AGr_L	Angular	Parietal lobe
33	PQ_R	73	PQ_L	Precuneus	Parietal lobe
34	PCL_R	74	PCL_L	Paracentral	Frontal lobe
35	HES_R	75	HES_L	Heschl	Temporal lobe
36	T1_R	76	T1_L	Superior temporal gyrus	Temporal lobe
37	T1P_R	77	T1P_L	Temporal pole: superior temporal gyrus	Limbic lobe
38	T2_R	78	T2_L	Middle temporal gyrus	Temporal lobe
39	T2P_R	79	T2P_L	Tem poral pole: middle temporal gyrus	Limbic lobe
40	T3_R	80	T3_L	Inferior temporal gyrus	Temporal lobe

Fig. 1. Structural connectivity of the brain. (A) The connectivity strength matrix (the connectivity strength is normalized so that the maximal strength is 1). (B) The fiber length matrix (mm). (C) The list of anatomical areas of interests. There are 40 different anatomical areas of interests, and each appears in both hemispheres. In the table, each row corresponds to an anatomical area, and the columns show the index and label of the area in the right hemisphere (RH), the index and label of the area in the left hemisphere (LH), the name of the area, and the corresponding anatomical region it belongs to.

connectivity strength and fiber length are set to 0 ($\mathbf{C}_{pp}=0, \mathbf{L}_{pp}=0, p=1,\ldots,P$). The order of brain areas in both matrices is arranged according to the index of brain areas in Fig. 1(C).

Graph theory methods

Centrality is a structural attribute of nodes in a network, which measures how central an actor is in network, and the contribution of network position to the importance, influence, prominence of an actor in a network. Central nodes in a network are those that have structural or functional importance. To explore the centrality, we compute two measures for all nodes: degree centrality and betweeness centrality, which have been used to study the structural connectivity of the brain (Ghosh et al., 2008; Honey et al., 2007). In this study, both measures are computed based on the connectivity strength matrix **C**.

Degree centrality is defined as the number of links incident upon a node (i.e., the number of ties that a node has). The degree centrality of a brain area is computed based on the connectivity strength matrix **C**. As the matrix **C** is symmetric, the degree of the *pth* brain area is computed as the sum of the elements in the *pth* row $deg_p=\sum_{q=1}^{P}\mathbf{C}_{pq}$, $p=1,\ldots,P$.

Betweenness centrality is the fraction of all shortest paths (a path between two nodes in a graph such that the sum of the weights of its constituent edges is minimized) in the network that contain a given node. Nodes with high values of betweenness centrality participate in a large number of shortest paths. The betweenness centrality is calculated by using the Matlab toolbox (http://www.brain-connectivity-toolbox.net), which is specially developed for complex network measures of brain connectivity (Rubinov and Sporns, 2010).

Neural dynamics model

We simulate the neural activity on a network of N nodes defined using the previously described structural connectivity: the connection strength matrix **C** (normalized so that the maximal strength is 1) and the fiber length matrix **L**. For convenience, we first transform the fiber length matrix **L** into a conductance delay matrix **T** by a choice of a conduction velocity v = 1 m/s such that **T** = **L**. As the maximal fiber length in **L** is 139 mm, the maximal conductance delay in **T** is 139 ms.

Different from exiting works (Cabral et al., 2011; Deco et al., 2009, 2011; Ghosh et al., 2008; Honey et al., 2007, 2009), in which the neural dynamics at each brain area is modeled by a single neural oscillator (FitzHugh–Nagumo oscillator, Wilson–Cowan oscillator, etc), we use a system of coupled phase oscillators described by Kuramoto (1984) models to represent neural dynamics at each local brain area. Therefore, the proposed model is capable of representing not only the synchronization on a global level but also local synchronization on a specific brain area. Synchronization phenomena in large populations of interacting elements have been intensively studied in physical, biological, chemical, and social systems. The Kuramoto model (Acebron, 2005; Kuramoto, 1984) is a successful approach to the problem of synchronization, in which each member of the population is described as a phase oscillator running at arbitrary intrinsic frequencies and those oscillators are coupled through the sine of their phase differences. While simple enough to be mathematically tractable, the model is sufficiently complex to be nontrival, rich enough to display a large variety of synchronization patterns, and sufficiently flexible to be adapted to many different contexts.

The Kuramoto model has been used to study oscillatory brain activity and several extensions have been proposed that increase its neurobiological plausibility, for instance by incorporating topological properties of local cortical connectivity (Breakspear et al., 2010). In particular, it describes how the activity of a group of interacting neurons can become synchronized and generate large-scale oscillations (Kitzbichler et al., 2009). Simulations using the Kuramoto model with realistic long-range cortical connectivity and time-delayed interactions reveal the emergence of slow patterned fluctuations that reproduce resting-state BOLD functional maps, which can be measured using fMRI (Cabral et al., 2011).

The dynamics of the Kuramoto model consisting of a population of *N* coupled phase oscillators is governed by (Acebron, 2005)

$$\dot{\theta}_n(t)=\omega_n+\sum_{j=1}^{N}k_{nj}sin\left(\theta_j\left(t-\tau_{nj}\right)-\theta_n(t)\right), n=1,\ldots,N, \tag{1}$$

where $\theta_n(t)$ is the phase of the *nth* oscillator at time *t*, $f_n=\omega_n/2\pi$ is the intrinsic frequency of the *nth* oscillator, k_{nj} and τ_{nj} are the coupling strength and conductance delay from *jth* oscillator to *nth* oscillator.

In this study, we assume all the oscillators have the same intrinsic frequency

$$f_n=f, n=1,\ldots,N, \tag{2}$$

and use *f* as a global parameter to study the occurrence of synchronization at different frequencies. If the *nth* oscillator and the *jth* oscillator are from the *pth* and the *qth* brain areas, respectively, then

$$k_{nj}=S_{global}\mathbf{C}_{pq}\quad \tau_{nj}=S_{delay}\mathbf{T}_{pq}, \tag{3}$$

where $\mathbf{C}_{pq}$ and $\mathbf{T}_{pq}$ are the elements of the *pth* row and *qth* column of the matrices **C** and **T**, and S_{global} and S_{delay} are the scaling factors. Therefore, the connectivity and the delay matrices are fixed in their structure and only their scaling can be varied with S_{global} and S_{delay}, respectively. If the two oscillators are from the same brain area, then

$$k_{nj}=S_{local}\quad \tau_{nj}=0, \tag{4}$$

where S_{local} is the scaling factor for local coupling strength. So each oscillator connects to all other local oscillators within each brain area. As the current study is focused on the role of global connectivity, we assume the local coupling strength is the same for all brain areas and the local time delay is 0.

At the global level, the network synchrony can be evaluated by a complex-valued global order parameter defined by

$$R(t)e^{i\phi(t)}=\frac{1}{N}\sum_{n=1}^{N}e^{i\theta_n(t)}, \tag{5}$$

where the amplitude $R(t)$ measures phase uniformity and varies between 0 for a fully desynchronized or incoherent state to 1 for a fully synchronized state. For sufficient synchrony, the phase $\phi(t)$ describes the movement of the oscillator ensemble around the unit circle.

At the local level, the network synchrony for each brain area can be evaluated similarly. For example, if there are *P* brain areas and *M* oscillators in each area, the local order parameter for the *pth* area is defined as follows

$$R_p(t)e^{i\phi_p(t)}=\frac{1}{M}\sum_{m=1}^{M}e^{i\theta_{m(p)}(t)}, p=1,\ldots,P, \tag{6}$$

where $\theta_{m(p)}(t)$ represents the phase of the *pth* oscillator in the *mth* brain area. As all the brain areas have the same number of oscillators in the current model, the global parameter is the average of the local order parameters

$$R(t)e^{i\phi(t)}=\frac{1}{P}\sum_{p=1}^{P}R_p(t)e^{i\phi_p(t)}. \tag{7}$$

The present model depends on four independent parameters: scaling factor of global coupling strength S_{global}, scaling factor of local coupling strength S_{local}, scaling factor of global delay S_{delay}, and intrinsic frequency *f*. In this work, we conduct a set of partial

parametric studies in the 4 dimensional space (S_{global},S_{local},S_{delay},f). We first explore the 3 dimensional subspace (S_{global},S_{local},S_{delay}) by choosing an intrinsic frequency $f=4$ Hz. In the first step, we study the role of structural connectivity in the global synchronization in the delta range, which may correspond to the hypersynchronized oscillations in SW epileptic seizures. In the second step, we explore the 3 dimensional subspace (S_{global},S_{local},f) by choosing a scaling factor $S_{delay}=0.1$ for time delays. This scaling factor corresponds to a conductance speed of 10 m/s, which is in the physiologically realistic range of propagation velocity (around 5–20 m/s) for the adult primate brain (Ghosh et al., 2008). In this step, we study the influence of intrinsic frequencies on the global synchronization.

In this study, there are 80 brain areas ($P=80$) and there are 4 oscillators in each area ($M=4$). Therefore, the total number of oscillators is 328 ($N=328$). The system of N dynamical equations was numerically solved with a time-step 0.1 ms using forward Euler scheme. In each simulation, phases of oscillators in each brain area are initialized to be uniformly distributed on the interval [-π,π]. As a result, the amplitudes of the global and local order parameters equal zero $R(0)=0$, $R_p(0)=0$, $P=1,\ldots P$, and the whole network is initialized in a state of fully desynchronized or incoherence.

The simulator is implemented in C++ on a 24-core PowerEdge R715 machine with 2 AMD Operton 2.2 GHz 12-core processors and 32 GB RAM. The simulation results are processed and visualized in Matlab. Especially, the BrainNET Viewer (http://www.nitrc.org/projets/bnv/) is used to visualize the brain network.

Results

Identification of the central nodes

Central nodes in a network are those that have structural or functional importance. To explore the centrality, we compute degree centrality and betweenness centrality for all the brain areas (Methods). A brain view of connectivity, degree centrality, and betweenness centrality is shown in Fig. 2(A). The figure includes sagittal, axial, and coronal views of both hemispheres of the brain. The color of nodes represents degree centrality (which decreases from deep red to deep blue) and the size of nodes represents betweenness centrality. The size of edges connecting two nodes represents the strength of connectivity. Degree centrality and betweenness centrality of brain areas are also compared in the bar graphs in Figs. 2(B) and (C), respectively.

The top twenty brain areas for degree centrality and betweenness centrality are listed in Figs. 2(E) and (F), respectively. For degree centrality, the top five areas are right dorsolateral part of superior frontal gyrus (F1_R), left dorsolateral part of superior frontal gyrus (F1_L), left middle occipital gyrus (O2_L), right supplementary motor ares (SMA_R), and right middle frontal gyrus (F2_R). For betweenness centrality, the top five areas are left dorsolateral part of superior frontal gyrus (F1_L), right dorsolateral part of superior frontal gyrus (F1_R), left middle frontal gyrus (F2_L), right middle frontal gyrus (F2_R), and right middle temporal gyrus (T2_R).

Among those brain areas, right dorsolateral part of superior frontal gyrus (F1_R), left dorsolateral part of superior frontal gyrus (F1_L), and right middle frontal gyrus (F2_R) are highly ranked across both measures, and can be identified as structural hubs in terms of centrality. Conceptually similar to an airline hub, these are brain areas with a comparatively high number of connections to the rest of the network. As we will demonstrate below, the structural hubs have consequences on the initialization of global synchronization.

Roles of coupling strengths and conduction delays in the emergence of global synchronization

As briefly mentioned in Methods, the present model depends on four free parameters: scaling factor of global coupling strength S_{global}, scaling factor of local coupling strength S_{local}, scaling factor of global delay S_{delay}, and intrinsic frequency f. In this work, we conduct a set of partial parametric studies in the 4 dimensional space (S_{global},S_{local},S_{delay},f).

In this part, we explore the 3 dimensional subspace (S_{global},S_{local},S_{delay}) by choosing an intrinsic frequency $f=4$ Hz to study the role of structural connectivity in the global synchronization in the delta range. Such synchronization may correspond to the hypersynchronized oscillations in SW epileptic seizures. The ranges of the three parameters are as follows: $S_{global}\in[0,1]$, $S_{local}\in[0,1]$, and $S_{delay}\in[0,1]$. As a result, in the range of parameters, all coupling strengths are smaller than 1. The range of coupling strengths is selected based on the following two reasons: first, the coupling strength is sufficiently small to make sure the phase reduction remains valid (Breakspear et al., 2010); second, the range is sufficiently large to unveil the roles of parameters of interests qualitatively. The maximal scaling factor of the delay $S_{delay}=1$ corresponds to the smallest conductance velocity $v=1$ m/s, and thus the range of delays covers the physiologically realistic range of propagation velocities for the adult primate brain (around 5–20 m/s) (Ghosh et al., 2008). For each set of parameter combination (S_{global},S_{local},S_{delay}), the whole network is initialized in a fully desynchronized state, and simulated for 10 seconds so that steady state can be approached in most cases. Note that, similar qualitative results can be found by repeating the simulation for different instantiations of the initial conditions. The amplitude of global order parameter at the final moment $R(10)$ is used as the measure of global synchronization.

As shown in Fig. 3, the 3 dimensional parameter space is demonstrated as a set of 2 dimensional plane corresponding to different time delays. In Figs. 3(A)–(F), the scaling factors of time delays are $S_{delay}=0$(A), $S_{delay}=0.1$(B),$S_{delay}=0.2$(C),$S_{delay}=0.3$(D), $S_{delay}=0.4$(E), and $S_{delay}=0.5$(F). The corresponding conductance velocities are $v=0$ m/s (A), $v=10$ m/s (B), $v=5$ m/s (C),$v=3.33$ m/s (D), $v=2.5$ m/s (E), and $v=2$ m/s (F). In Figs. 3(A)–(F), X-axis represents the scaling factor of local coupling strength S_{local}, Y-axis represents the scaling factor of global coupling strength S_{global}, and the color represents the degree of global synchronization. In Figs. 3(A)–(F), we see not only coupling strengths can play an important role in the emergence of global synchronization but also time delays can substantially change the dynamical properties of brain networks.

First, as shown in Figs. 3(A)–(F), the global synchronization is highly dependent on the time delays. In particular, the degree of global synchronization is decreased as the time delay increases. This means time delays tend to break coherence in populations of interacting units. Intuitively, this can be explained as follows: when all the oscillators oscillate in a synchronous fashion at the same frequency, the couplings reinforce synchronous in-phase oscillation without conductance delay; however, if conductance delay becomes nonzero, the stable synchronous oscillation may become unstable because the transmitted signal from one oscillator may arrive during the anti-phase of the other oscillator. Note that, the physiologically realistic range of propagation velocities is around 5—20 m/s for the adult primate brain (Ghosh et al., 2008). Therefore, the results in Figs. 3(B) and (C) fall into this physiological range as $S_{delay}=0.1$ and $S_{delay}=0.2$ correspond to $v=10$ m/s and $v=5$ m/s, respectively. Our results show that the state of global synchronization does exist in the physiological range and tends to vanish for longer delays $S_{delay}>0.3$.

Second, the relationship between global synchronization and coupling strength becomes more complex in the presence of time delays. In Fig. 3(A), when there is no delay, the relationship between two coupling strength in terms of global synchronization is straightforward: the global synchronization increases as either global or local coupling strength increases while the other is constant. Intuitively, one might think that an increase of coupling strength will always lead to a higher degree of global synchronization, but this might not be the case when time delays exist. For example, as shown in Figs. 3(B)–(F), the highest degree of global synchronization does not occur when both global and local coupling strength are maximal. In

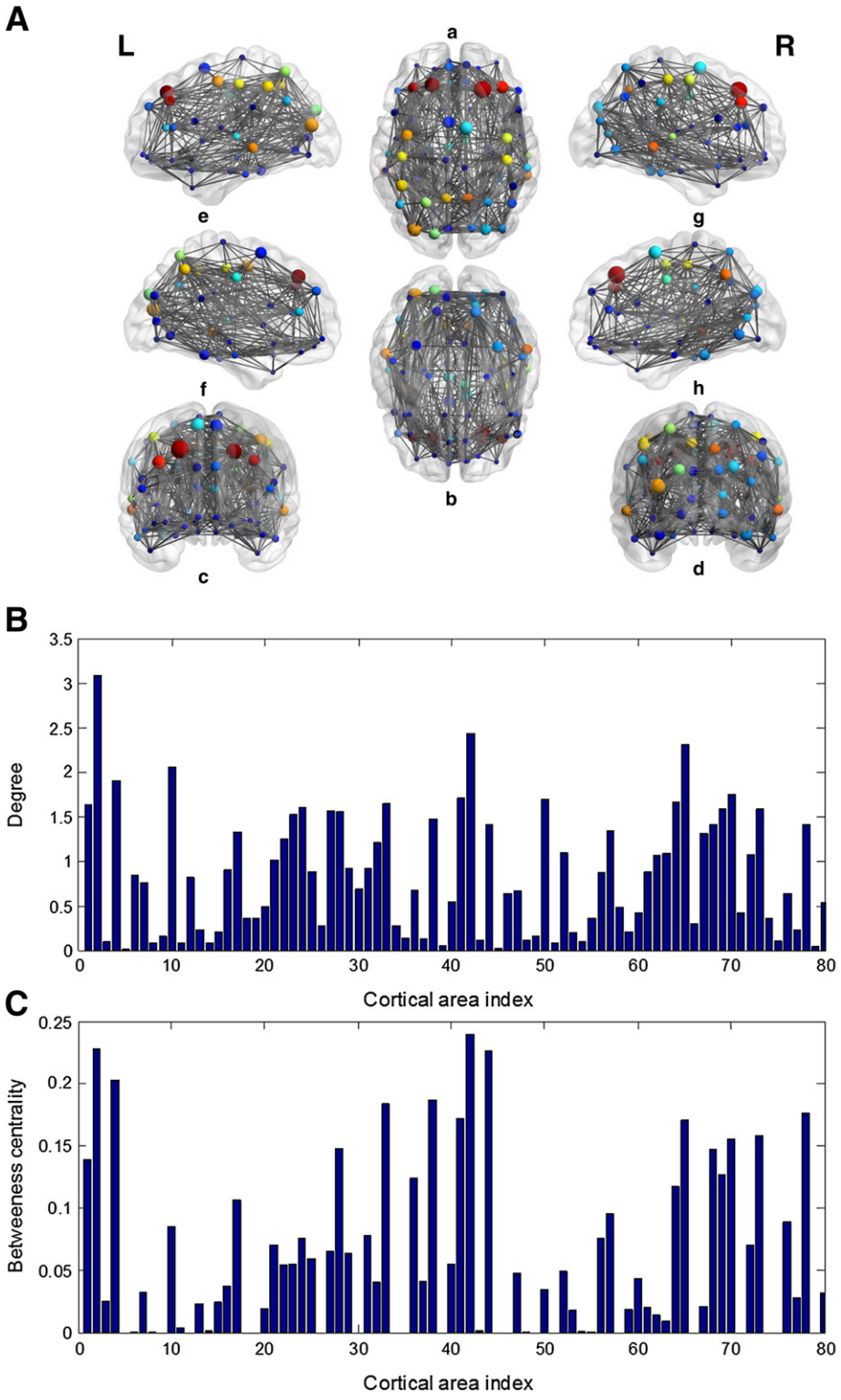

D

Degree

Rank	Area	Value
1	F1_R	3.0904
2	F1_L	2.4314
3	O2_L	2.3157
4	SMA_R	2.0543
5	F2_R	1.9038
6	P2_L	1.7542
7	PRE_L	1.7136
8	SMA_L	1.7006
9	O1_L	1.6723
10	PQ_R	1.6479
11	PRE_R	1.6421
12	O1_R	1.6089
13	PQ_L	1.5904
14	P1_L	1.5855
15	FUSI_R	1.5614
16	POST_R	1.5608
17	LING_R	1.5263
18	T2_R	1.4698
19	T2_L	1.4142
20	POST_L	1.4132

E

Betweeness centrality

Rank	Area	Value
1	F1_L	0.2395
2	F1_R	0.2278
3	F2_L	0.2262
4	F2_R	0.2032
5	T2_R	0.1866
6	PQ_R	0.184
7	T2_L	0.1762
8	PRE_L	0.1723
9	O2_L	0.1704
10	PQ_L	0.1581
11	P2_L	0.1555
12	POST_R	0.148
13	POST_L	0.1474
14	PRE_R	0.1392
15	P1_L	0.1266
16	T1_R	0.1237
17	O1_L	0.1172
18	MCIN_R	0.1061
19	MCIN_L	0.0951
20	T1_L	0.0886

Fig. 2. Degree centrality and betweenness centrality. (A) A brain view of connectivity, degree centrality, and betweenness centrality. The figure includes sagittal, axial, and coronal views of both hemispheres of the brain: (a) axial top to bottom, (b) axial bottom to top, (c) coronal front to back, (d) coronal back to front, (e) sagittal left to right (left hemisphere), (f) sagittal right to left (left hemisphere), (g) sagittal right to left (right hemisphere), (h) sagittal left to right (right hemisphere). The color of nodes represents the degree centrality (which decreases from deep red to deep blue) and the size of nodes represents the betweenness centrality. The size of edges connecting two nodes represents the strength of connectivity. (B) The Y-axis represents degree centrality and the X-axis represents the index of brain area. (C) The Y-axis represents betweenness centrality and the X-axis represents the index of brain areas. (D) Top twenty ranked brain areas for degree centrality. (E) Top twenty ranked brain areas for betweenness centrality.

Fig. 3(C), the highest degree of global synchronization occurs in two disjoint sets. In contrast, in Figs. 3(B), (D), (E), and (F), the highest degree of global synchronization occurs only in one set, in which the global coupling strength is not maximal.

Overall, these results show that space–time structure of the coupling defined by the anatomical connectivity (space) and the time delays (time) can be the primary component contributing to the emergence of global synchronization. Those results may have direct

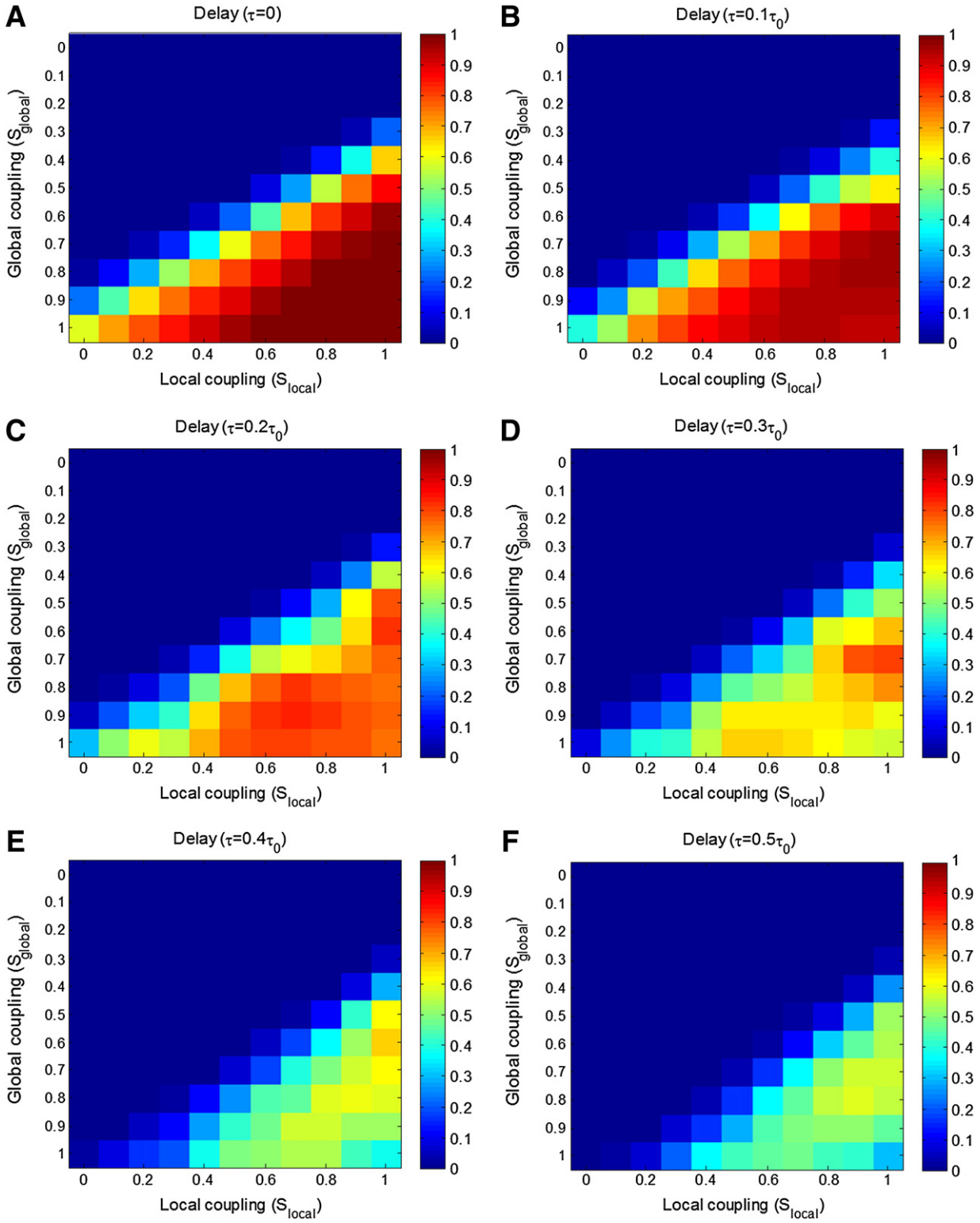

Fig. 3. Global synchronization in the parameter space of global and local coupling strength at different time delays. The X-axis represents the scaling factor of local coupling strength S_{local}, the Y-axis represents the scaling factor of global coupling strength S_{global}, and the color represents the amplitude of global order parameter. (A) Time delay $\tau = 0 (v = 0$ m/s). (B) Time delay $\tau = 0.1\tau_0 (v = 10$ m/s). (C) Time delay $\tau = 0.2\tau_0 (v = 5$ m/s). (D) Time delay $\tau = 0.3\tau_0 (v = 3.33$ m/s). (E) Time delay $\tau = 0.4\tau_0 (v = 2.5$ m/s). (F) Time delay $\tau = 0.5\tau_0 (v = 2$ m/s).

implications for studies of SW epileptic seizures. The SW epileptic seizures, different from localized seizure, are characterized by a sudden emergence of brain level synchronization. While the roles of cellular and synaptic mechanisms have been widely studied, the sudden emergence of synchronization in such a large scale brain network is still difficult to explain. In this regard, we hypothesize that the brain structural connection is possible to play an important role. For example, the role of time delays in global synchronization indicates that the abnormality of white matter might facilitate the emergence of SW epileptic seizures. The abnormality of the length, diameter, and

myelination of axons may contribute to the abnormality of the time delays. To verify the hypothesis, computational studies need to be carried out with imaging techniques to quantify white matter integrity of the patients suffering from SW epilepsy.

Roles of intrinsic frequencies in the emergence of global synchronization

Mathematically, how important time delays are for a population of coupled phase oscillators is dependent on the ratio of the time delay to the natural period of a typical oscillator. In the scenario of a brain network, an interesting question would be how intrinsic frequencies influence the degree of global synchronization. In other words, can global synchronization emerge at all intrinsic frequencies? To study the role of intrinsic frequency, we explore the 3 dimensional subspace (S_{global},S_{local},f) by choosing a scaling factor $S_{delay}=0.1$. This corresponds to a conductance speed of 10 m/s, which is in the physiologically realistic range of propagation velocity (around 5-20 m/s) for the adult primate brain (Ghosh et al., 2008). Similar to the previous case, for each parameter combination (S_{global},S_{local},f), the whole network is initialized in a fully desynchronized state, and simulated for 10 s. The amplitudes of global order parameters at $t=10$ s are used as the measure of global synchronization.

As shown in Fig. 4, the 3 dimensional parameter space is demonstrated as a set of 2 dimensional plane corresponding to different intrinsic frequencies. The intrinsic frequencies in Figs. 4(A)–(F) are 2 Hz, 4 Hz, 6 Hz, 8 Hz, 10 Hz, and 12 Hz, respectively. While longer conductance delay tends to break coherence in populations of interacting units, higher intrinsic frequencies have the same effects. The results in Fig. 4 demonstrate a decrease of global synchronization as the intrinsic frequency increases. In particular, global synchronization tends to emerge at frequencies less than 6 Hz. In Figs. 4(A) and (B), large areas in parameter space are found where a high degree of synchronization can be achieved. Starting from Fig. 4(C), the areas corresponding to high values of global synchronization significantly decreases. Especially, the global synchronization vanishes beyond 12 Hz in the parameter space. The observation that global synchronization tends to emerge at low frequencies may partially explain the low characteristic frequencies of SWD. More interestingly, this agrees well with existing experimental observations. While neural populations can exhibit oscillations in a wide range of frequency bands, global synchronization in the brain scale only occurs at low frequencies. Although long range synchronization at high frequencies (beta and gamma rhythms) does exist in separate parts of the brain (Varela et al., 2001), the scale of such synchronization is quite limited compared with the generalized synchronization in SW epileptic seizures.

Cortical local and global synchronization interplay in the emergence of global synchronization

In the previous sections, we have demonstrated the roles of coupling strength, time delay, and intrinsic frequency in the global synchronization of the brain network. Another important question is about the roles played by different brain areas in the initialization of the global synchronization. It is interesting to know whether the global synchronization is initialized from some particular brain areas. To answer this question, we choose a combination of parameter $S_{global}=1$, $S_{local}=1$, $S_{delay}=0.1(v=10$ m/s), and $f=4$ Hz to examine the time courses of global and local synchronization. Note that, similar qualitative results can be obtained with other combinations of parameters underlying global synchronization. In this study, we use local order parameters to characterize the local synchronization of each brain area and a global order parameter to characterize the global synchronization.

As shown in Fig. 5(A), the blue lines represent the amplitudes of local order parameters of brain areas, and the red line represents the amplitude of the global order parameter. The global synchronization starts from an increase of local synchronization of some brain areas, and increases significantly in hundreds of milliseconds. The time courses of the amplitudes of global and local order parameters agree with the experimental observations in (Amor et al., 2009), where the mean global and local synchronization time course across all 21 seizures is depicted. In terms of local synchronization, there is considerable variation among brain areas: some brain areas tend to get synchronized earlier than others.

To better demonstrate the time courses, we show snapshots of global and local order parameters at different times ($t=0$ s, $t=4$ s, $t=5$ s, $t=6$ s, $t=7$ s) in the polar coordinate system, where complex-valued order parameter is represented by a vector whose length is $R(t)$ and angle is $\phi(t)$. In Fig. 5(B), at $t=0$ s, all the order parameters are represented by the origin. This is because the phases of oscillators in each brain area are initialized to be uniformly distributed, and thus the amplitudes of all the order parameters equal zero at the beginning of the simulation. From $t=4$ s to $t=7$ s, we take snapshots every single second to demonstrate the emergence of synchronization at both local and global levels. In Fig. 5(C), at $t=4$ s, the maximal amplitude of local order parameters is only 10^{-5}, and all the brain areas are still fully desynchronized. In Fig. 5(D), at $t=5$ s, the maximal amplitude of local order parameters is increased to be 0.002, and some brain areas start to show a tendency toward local synchronization. Significant changes characterized by local synchronization of some brain areas start to occur at $t=6$ s. As shown in Fig. 5(E), at the local level, a few brain areas are in a state of partial synchronization, and the maximal amplitude of local order parameters is about 0.5. In contrast, at the global level, the network is still desynchronized as the amplitude of global order parameter is only 0.05. By the time $t=7$ s, as shown in Fig. 5(E), not only many brain areas have become locally synchronized but also the global synchrony level has increased substantially. The amplitude of the global order parameter is 0.66 and the network is partially synchronized at the global level. Overall, the above results show that the emergence of global synchronization starts from the emergence of local synchronization of a few brain areas.

Given the observation above, it is interesting to find out what brain areas are involved at the initialization stage of global synchronization and why. To answer this question, we further characterize the initialization of synchronization in both time and space. First of all, we study the spatial distribution of local synchronization events at $t=6$ s when global synchronization starts to emerge. As shown in Fig. 6(A), a brain view of the degree of local synchronization is given. The figure includes sagittal, axial, and coronal views of both hemispheres of the brain, where the color of nodes represents the amplitude of local order parameter (which decreases from deep red to deep blue), and the size of nodes represents the degree centrality. We see there is a strong correlation between the degree of local synchronization and the degree centrality: the nodes with deep red colors turn out to be the nodes of large sizes. To better demonstrate this, the amplitudes of local order parameters of brain areas are compared in Fig. 6(B), and the top twenty ranked brain areas are listed in Fig. 6(C).

In the initialization stage of global synchronization ($t=6$ s), the top five ranked areas are right dorsolateral part of superior frontal gyrus (F1_R), left dorsolateral part of superior frontal gyrus (F1_L), right supplementary motor areas (SMA_R), right middle frontal gyrus (F2_R), and left supplementary motor areas (SMA_L). Compared with the lists in Fig. 2(C), we see that the structural hubs identified (F1_R, F1_L, F2_R) are ranked in the first, second, and fourth places, respectively, in Fig. 6(C). This means global synchronization is initialized from a few "hot spots" corresponding to brain areas with highest degree of centrality. According to the anatomical regions defined in (Tzourio-Mazoyer et al., 2002), among the top twenty areas, 17 areas belong to frontal lobe: F1_R(1st), R1_L(2nd), SMA_R(3rd), F2_R(4th), SMA_L(5th), F1M_L(6th), F_L(7th), F1M_R(9th), F3T_R(10th), and F3OP_R(11th); 4 areas belong to central regions: PRE_R(8th),

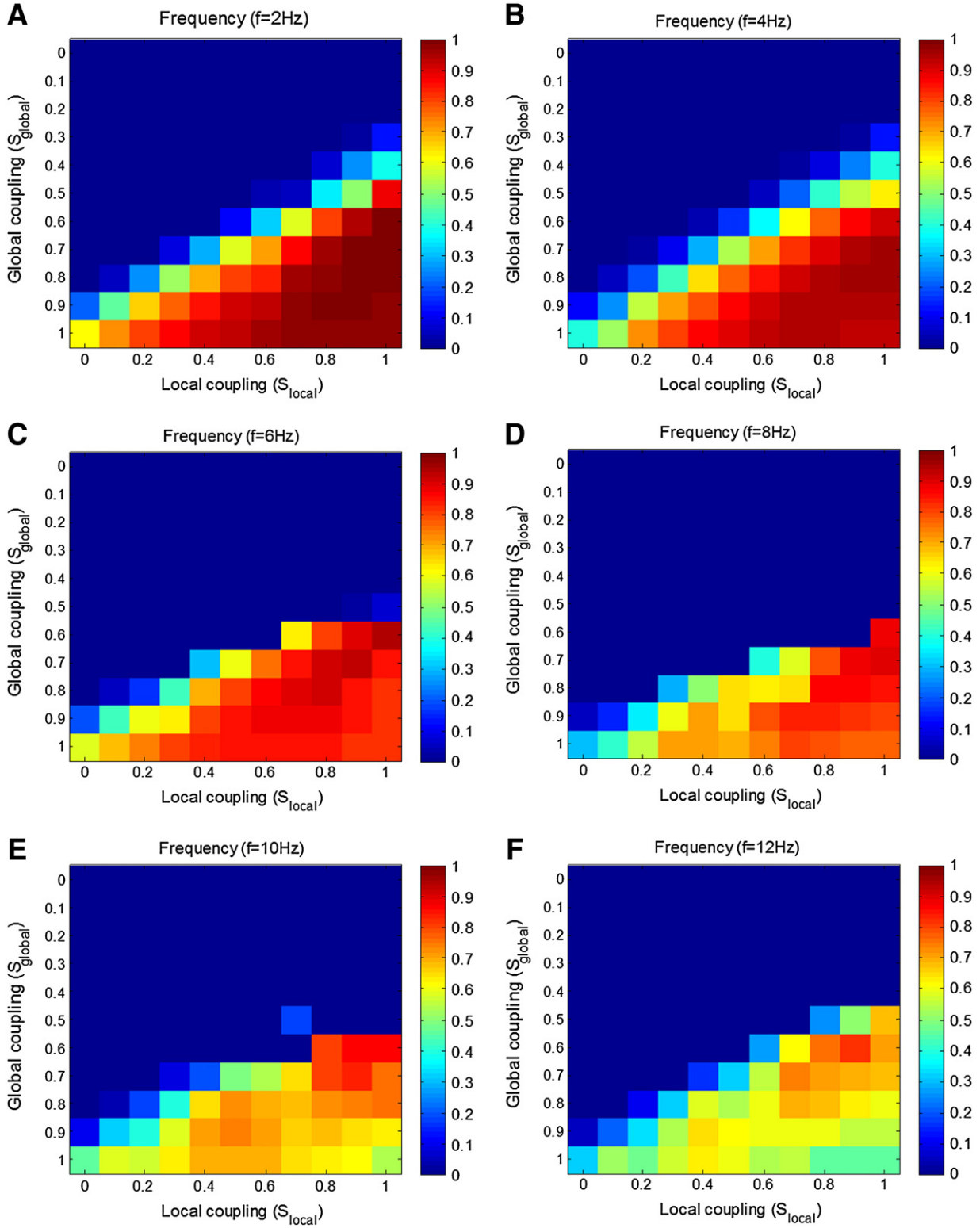

Fig. 4. Global synchronization in the parameter space of global and local coupling strength at different intrinsic frequencies. The X-axis represents the scaling factor of local coupling strength S_{local}, the Y-axis represents the scaling factor of global coupling strength S_{global}, and the color represents the amplitude of global order parameter. (A) Intrinsic frequency $f=$ 2 Hz. (B) Intrinsic frequency $f=4$ Hz. (C) Intrinsic frequency $f=6$ Hz. (D) Intrinsic frequency $f=8$ Hz. (E) Intrinsic frequency $f=10$ Hz. (F) Intrinsic frequency $f=12$ Hz.

PRE_L(12th), POST_R(15th), and POST_L(18th); 4 areas belong to limbic lobe: MCIN_L(13th), MCIN_R(14th), ACIN_R(16th), and ACIN_L(17th); only 1 area belongs to parietal lobe: P2_L(19th); only 1 area belongs to occipital lobe: O2_L(20th). Therefore, brain areas from frontal lobe are playing a dominant role in the initialization stage of the global synchronization. In addition to those frontal areas, precentral gyrus (PRE), postcentral gyrus (POST), median cingulate and paracingulate gyrus (MCIN), and anterior cingulate and paracingulate gyrus (ACIN) are also

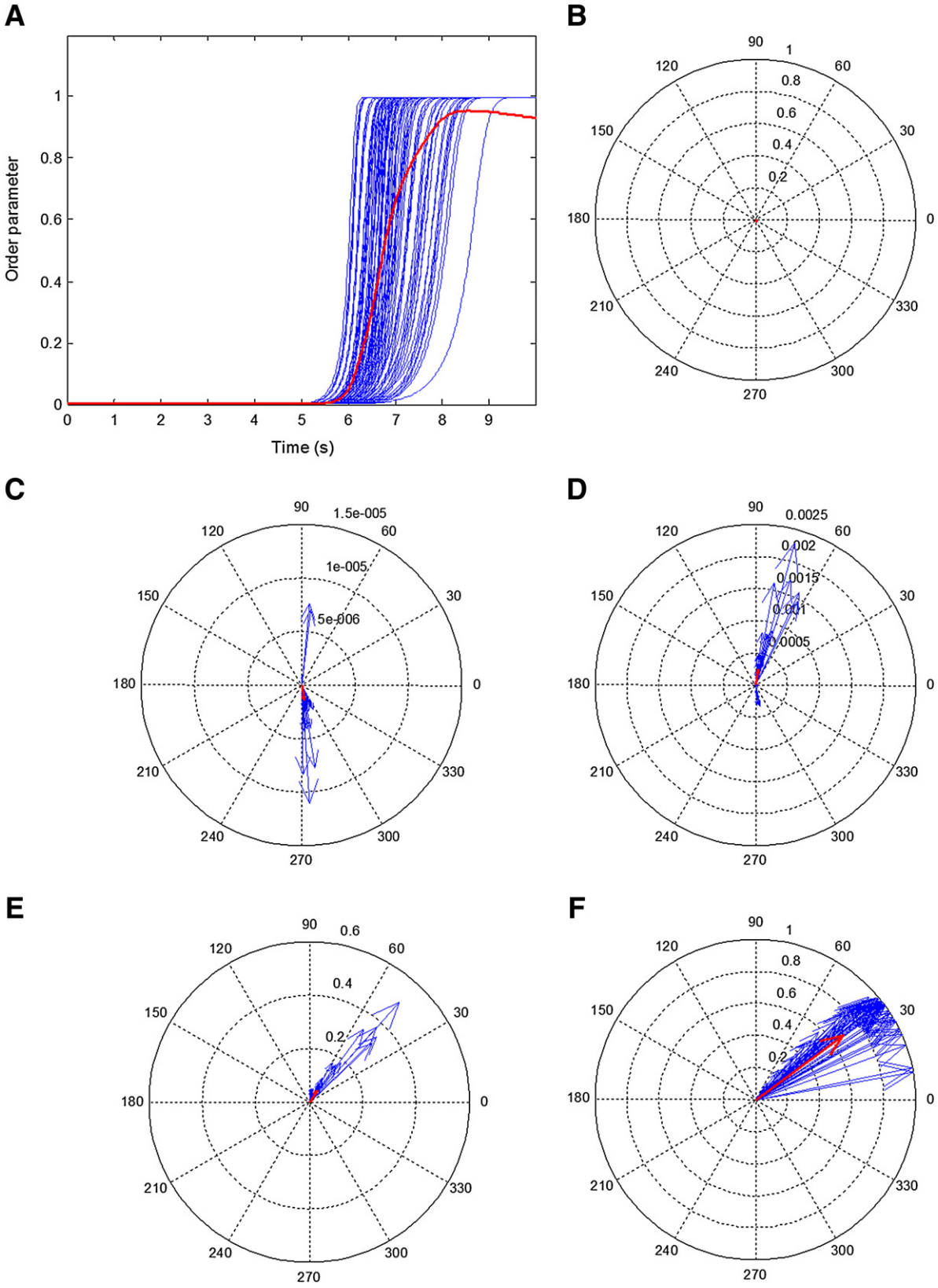

Fig. 5. The time courses of global and local synchronization. (A) The X-axis represents the time, and the Y-axis represents the amplitudes of order parameters. The blue lines represent the amplitudes of local order parameters of brain areas, and the red line represents the amplitude of the global order parameter. (B) The global (red) and local (blue) order parameters of brain areas in the polar coordinate system at $t=0$ s. (C) The global (red) and local (blue) order parameters of brain areas in the polar coordinate system at $t=4$ s. (D) The global (red) and local (blue) order parameters of brain areas in the polar coordinate system at $t=5$ s. (E) The global (red) and local (blue) order parameters of brain areas in the polar coordinate system at $t=6$ s.

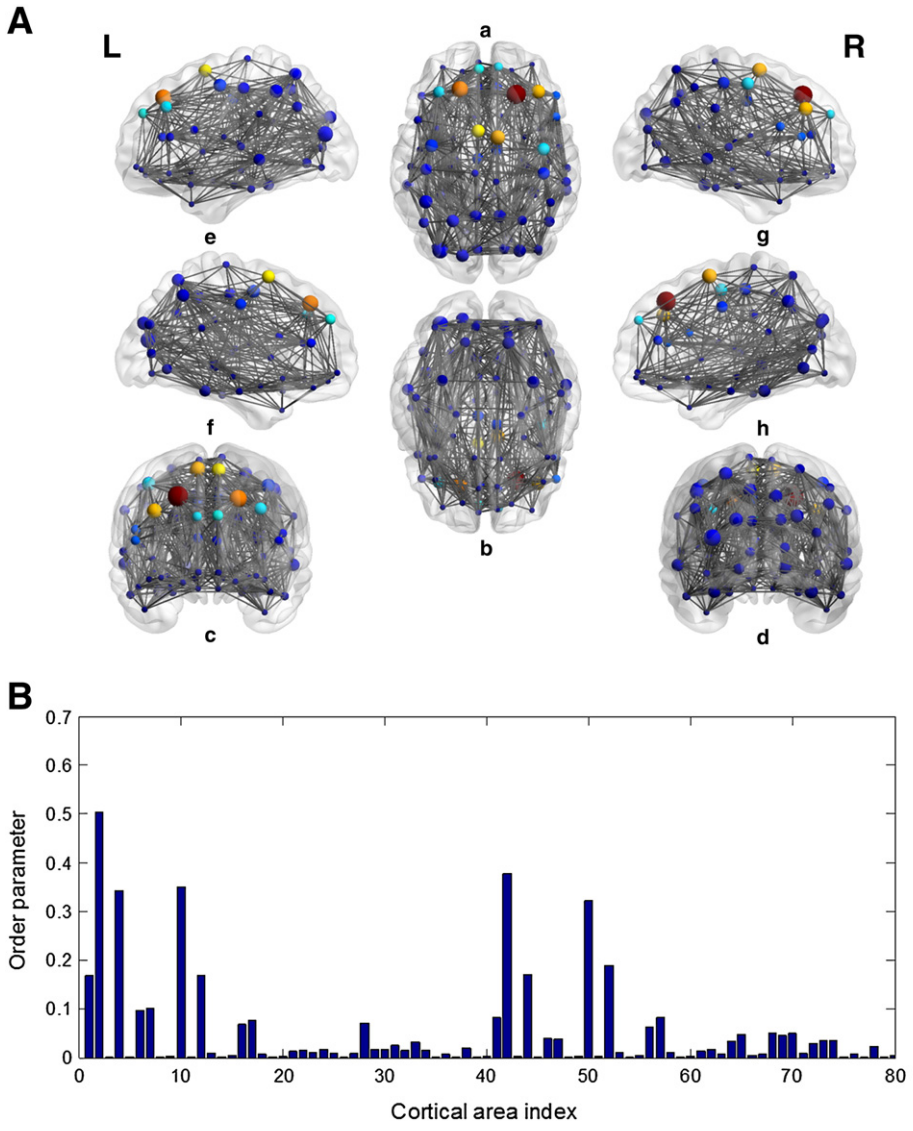

C

Order parameter (t=6s)

Rank	Area	Value
1	F1_R	0.505
2	F1_L	0.378
3	SMA_R	0.3516
4	F2_R	0.3426
5	SMA_L	0.3221
6	F1M_L	0.1889
7	F2_L	0.1708
8	PRE_R	0.1697
9	F1M_R	0.1687
10	F3T_R	0.1019
11	F3OP_R	0.0974
12	PRE_L	0.0832
13	MCIN_L	0.082
14	MCIN_R	0.0769
15	POST_R	0.0705
16	ACIN_R	0.0685
17	ACIN_L	0.0632
18	POST_L	0.051
19	P2_L	0.0495
20	O2_L	0.0479

Fig. 6. Spatial distribution of local synchronization events at $t=6$ s. (A) A brain view of the amplitudes of local order parameters of brain areas. The figure includes sagittal, axial, and coronal views of both hemispheres of the brain: (a) axial top to bottom, (b) axial bottom to top, (c) coronal front to back, (d) coronal back to front, (e) sagittal left to right (left hemisphere), (f) sagittal right to left (left hemisphere), (g) sagittal right to left (right hemisphere), (h) sagittal left to right (right hemisphere). The color of nodes represents the amplitude of local order parameters (which decreases from deep red to deep blue), the size of nodes represents the degree centrality, and the size of edges connecting two nodes represents the strength of connectivity. (B) The Y-axis represents the amplitude of local order parameter and the X-axis represents the index of brain area. (C) Top twenty ranked brain areas for the amplitudes of local order parameters.

involved in the initialization stage. Similarly, the spatial distribution of local synchronization events at $t=7$ s is shown in Fig. 7. Different from the previous case, at $t=7$ s, the amplitude of global order parameter has increased to 0.66, which means there is a substantial degree of global synchrony. In this stage, as shown in Figs. 7(A) and (B), a large number of brain areas have been fully synchronized at the local level. Among the top twenty ranked brain areas in Fig. **7**(C), 9 brain areas belong to frontal lobe. While frontal areas are still dominant at this stage, there is no doubt that more and more areas from other brain regions are catching up.

Instead of the classical view of sudden generalized synchronous activities in SW epilepsy, our results are in favor of the alternative hypothesis that initiation of SW epileptic seizure originates from specific brain areas. The observation is largely in agreement with experimental studies based on brain imaging techniques (Amor et al., 2009; Holmes et al., 2004; Pavone and Niedermeyer, 2000). For example, a study by Holmes et al. (2004) used high density EEG combined with an inverse problem algorithm suggests that the initial SW had a clear anterior origin involving discrete focal regions of the frontal lobe (including dorsolateral, orbital and cingulum areas). By graph theory analysis, we believe that the frontal focus of SW epileptic seizures can be explained by the structural connectivity as well.

Reproducibility on a biologically realistic primate brain connectivity

In this section, to show the principal findings can be replicated, we perform analysis on a biologically realistic primate brain connectivity with different parcellation. The primate brain connectivity was obtained from the CoCoMac database (Kotter, 2004), and has been successfully used to study the role of space–time structure of brain connectivity in the fluctuation of resting state networks (Ghosh et al., 2008). The connectivity matrix of a single hemisphere collated from macaque tracing studies comprises 38 nodes with weights ranging from 0 to 3.

The 36 cortical areas are listed in Fig. 8(A) (two thalamic nucleus omitted). The connectivity matrix is shown in Fig. 8(B), where connectivity strength is normalized so that the maximal strength is 1. To quantitatively explore the connectivity characteristics, we compute degree

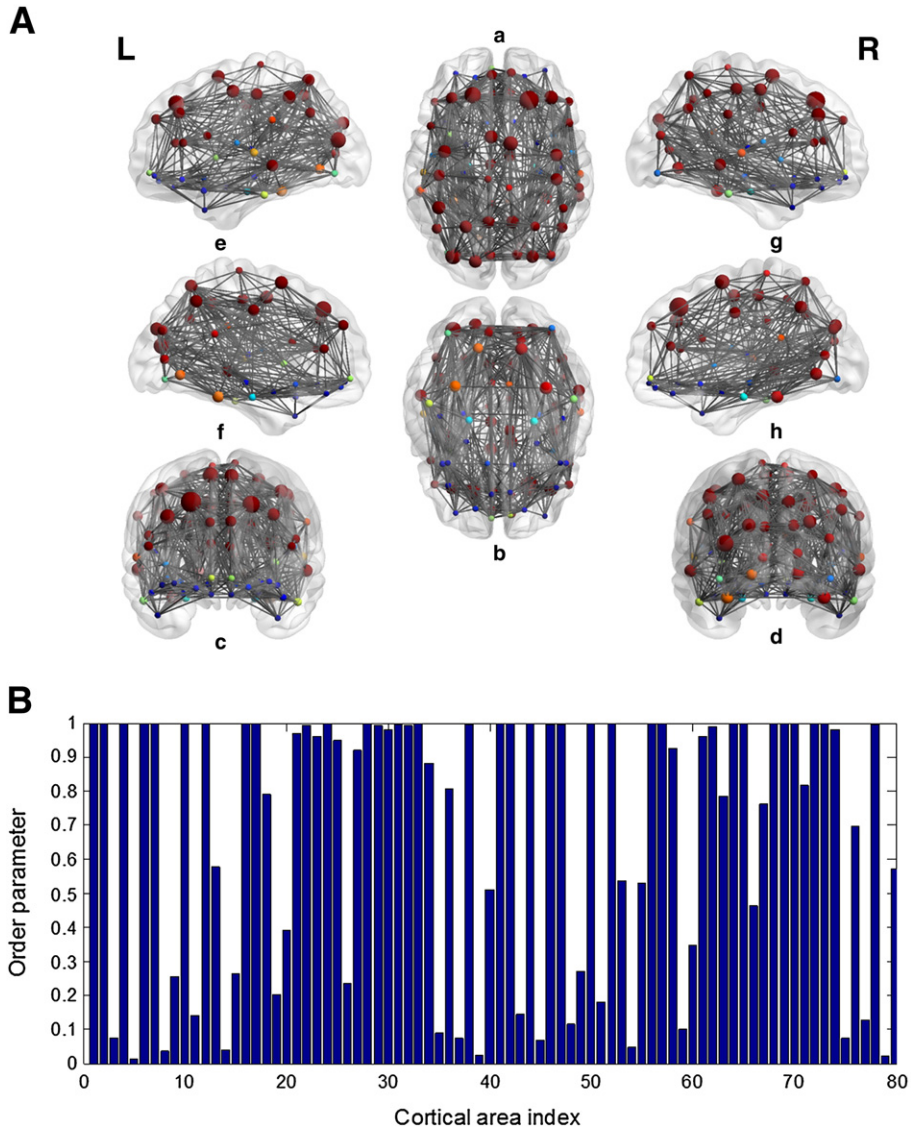

C

Order parameter (t=7s)

Rank	Area	Value
1	PRE_R	1
1	F1_R	1
1	F2_R	1
1	SMA_R	1
1	F1_L	1
1	SMA_L	1
1	F2_L	1
1	F1M_L	1
1	PRE_L	1
1	F1M_R	1
1	MCIN_L	1
1	POST_R	1
1	MCIN_R	1
1	O2_L	1
1	P2_L	1
16	POST_L	0.9999
16	F3OP_R	0.9999
16	P1_L	0.9999
16	F3T_R	0.9999
20	PQ_L	0.9998

Fig. 7. Spatial distribution of local synchronization events at $t = 7$ s. (A) A brain view of the amplitudes of local order parameters of brain areas. The figure includes sagittal, axial, and coronal views of both hemispheres of the brain: (a) axial top to bottom, (b) axial bottom to top, (c) coronal front to back, (d) coronal back to front, (e) sagittal left to right (left hemisphere), (f) sagittal right to left (left hemisphere), (g) sagittal right to left (right hemisphere), (h) sagittal left to right (right hemisphere). The color of nodes represents the amplitude of local order parameters (which decreases from deep red to deep blue), the size of nodes represents the degree centrality, and the size of edges connecting two nodes represents the strength of connectivity. (B) The Y-axis represents the amplitude of local order parameter and the X-axis represents the index of brain area. (C) Top twenty ranked brain areas for the amplitudes of local order parameters.

centrality and betweenness centrality of cortical areas, and the results are shown in the bar graphs in Figs. 8(C) and (D), respectively. The top ten brain areas for degree centrality and betweenness centrality are also listed. For degree centrality, the top five areas are PFCORB, PFCCL, PFCVL, PCIP, and TCS. For betweenness centrality, the top five areas are PFCORB, PFCCL, PCI, CCA, and TCS. Among those brain areas, PFCORB (orbital prefrontal cortex) and PFCCL (centrolateral prefrontal cortex) are highly ranked across both measures, and can be identified as structural hubs in terms of centrality.

To evaluate the temporal aspect of the coupling, the time delay between any two coupled network nodes is estimated as the ratio d/v, where d is Euclidean distance between two nodes in the three-dimensional physical space and v the propagation velocity (Ghosh et al., 2008). As realistic fiber tracking would generally result in longer pathways than the estimated shortest distance, the estimated time delay represents a lower estimate.

We demonstrate the roles of coupling strengths, time delays, and intrinsic frequencies in the emergence of global synchronization in Figs. 9(A)–(F), where X-axis represents the scaling factor of local coupling strength S_{local}, Y-axis represents the scaling factor of global coupling strength S_{global}, and the color represents the degree of global synchronization. First, to study the influence of time delays on the global synchronization, we explore the 3 dimensional subspace (S_{global},S_{local}, S_{delay}) by choosing an intrinsic frequency $f = 4$ Hz. As shown in Figs. 9(A)–(C), the scaling factors of time delays are $S_{delay} = 0$(A), $S_{delay} = 0.2$(B), and $S_{delay} = 0.4$(C), respectively. As the time delay increases, the degree of global synchronization is decreased. Second, to study the influence of intrinsic frequencies on the global synchronization, we explore the 3 dimensional subspace (S_{global},S_{local},f) by choosing a scaling factor $S_{delay} = 0.1$ for time delays. The intrinsic frequencies in Figs. 9(D)–(F) are 4 Hz, 8 Hz, and 12 Hz, respectively. It is clear that higher intrinsic frequencies have the same effects as longer time delays.

A List of cortical areas

Index	Abbreviation	Coritcal area name
1	A1	Primary auditory
2	A2	Secondary auditory
3	CCA	Anterior cingulate cortex
4	CCP	Posterior cingulate cortex
5	CCR	Retrosplenial cingulate cortex
6	CCS	Subgenual cingulate cortex
7	FEF	Frontal eye field
8	IA	Anterior insula
9	IP	Posterior insula
10	M1	Primary motor cortex
11	PCI	Inferior parietal cortex
12	PCIP	Intraparietal sulcus cortex
13	PCM	Medial parietal cortex
14	PCS	Superior parietal cortex
15	PFCCL	Centrolateral prefrontal cortex
16	PFCDL	Dorsolateral prefrontal cortex
17	PFCDM	Dorsomedial prefrontal cortex
18	PFCM	Medial prefrontal cortex
19	PFCORB	Orbital prefrontal cortex
20	PFCPOL	Prefrontal polar cortex
21	PFCVL	Ventrolateral prefrontal cortex
22	PHC	Parahippocampal cortex
23	PMCDL	Dorsolateral premotor cortex
24	PMCM	Medial (supplementary) remotor cortex
25	PMCVL	Ventrolateral premotor cortex
26	S1	Primary somatosensory cortex
27	S2	Secondary somatosensory cortex
28	TCC	Central temporal cortex
29	TCI	Inferior temporal cortex
30	TCPOL	Polar temporal cortex
31	TCS	Superior temporal cortex
32	TCV	Ventral temporal cortex
33	V1	Primary visual cortex
34	V2	Secondary visual cortex
35	VACD	Dorsal anterior visual cortex
36	VACV	Ventral anterior visual cortex

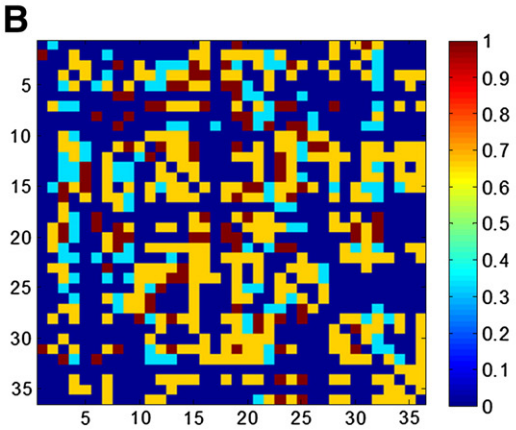

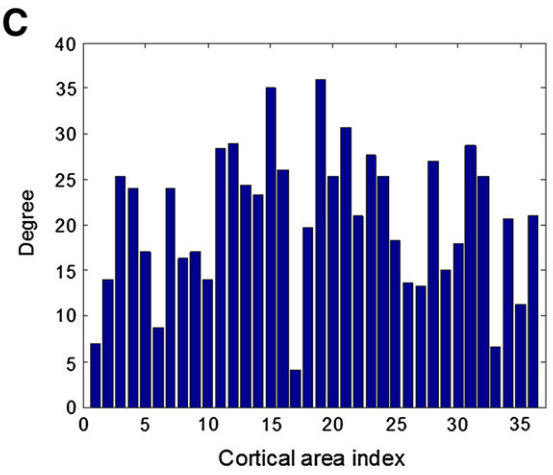

Degree

Rank	Area	Value
1	PFCORB	36
2	PFCCL	35
3	PFCVL	30.6667
4	PCIP	29
5	TCS	28.6667
6	PCI	28.3333
7	PMCDL	27.6667
8	TCC	27
9	PFCDL	26
10	CCA	25.3333

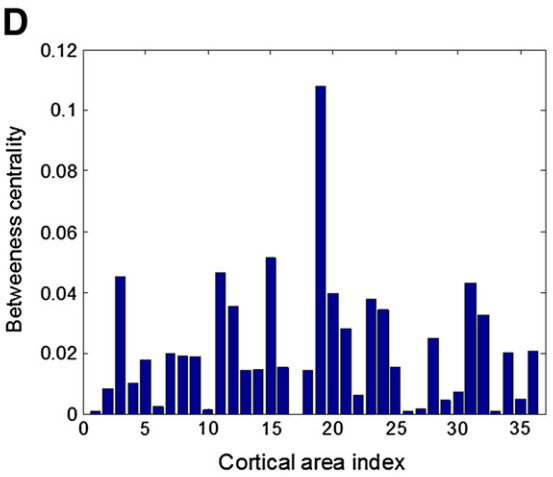

Betweeness centrality

Rank	Area	Value
1	PFCORB	0.1077
2	PFCCL	0.0513
3	PCI	0.0465
4	CCA	0.0451
5	TCS	0.0431
6	PFCPOL	0.0395
7	PMCDL	0.0377
8	PCIP	0.0354
9	PMCM	0.0343
10	TCV	0.0323

Fig. 8. Structural connectivity of the brain. (A) The list of anatomical areas of interests. There are 36 different anatomical areas of interests. In the table, each row corresponds to an anatomical area, and the columns show the index and label of the area, and the name of the area. (B) The connectivity strength matrix (the connectivity strength is normalized so that the maximal strength is 1). (C) The Y-axis represents degree centrality and the X-axis represents the index of brain area. Top ten ranked brain areas for degree centrality are listed in the table. (D) The Y-axis represents betweenness centrality and the X-axis represents the index of brain areas. Top ten ranked brain areas for betweenness centrality are listed in the table.

To examine the time courses of global and local synchronization, we choose a combination of parameter $S_{global}=0.1$, $S_{local}=1$, $S_{delay}=0.1$, and $f=4Hz$. As shown in Fig. 10(A), the global synchronization starts from an increase of local synchronization of some brain areas, and increases significantly in hundreds of milliseconds. The snapshots of global and local order parameters at $t=7$ s and $t=7.5$ s are shown in the polar coordinate system in Figs. 10(B) and (D). During early stage of initialization, at $t=7$ s, the degree of synchronization is relatively small at both global and local levels. The maximal amplitude of local order parameters is 0.1389, and the amplitude of global order parameter is 0.0775. However, by the time $t=7.5$ s, as shown in Fig. 10(D), many brain areas have become locally synchronized, and the amplitude of global order parameter has increased substantially to 0.6256.

To demonstrate the correlation between the degree of local synchronization and the degree centrality, the amplitudes of local order parameters of brain areas at $t=7$ s and $t=7.5$ s are compared in Figs. 10(C)(E) and the top ten ranked brain areas are listed. In both snapshots, the top five ranked areas are PFCORB, PFCCL, PFCVL, PMCDL, and PMCM. Compared with the lists in Fig. 8, we see that the structural

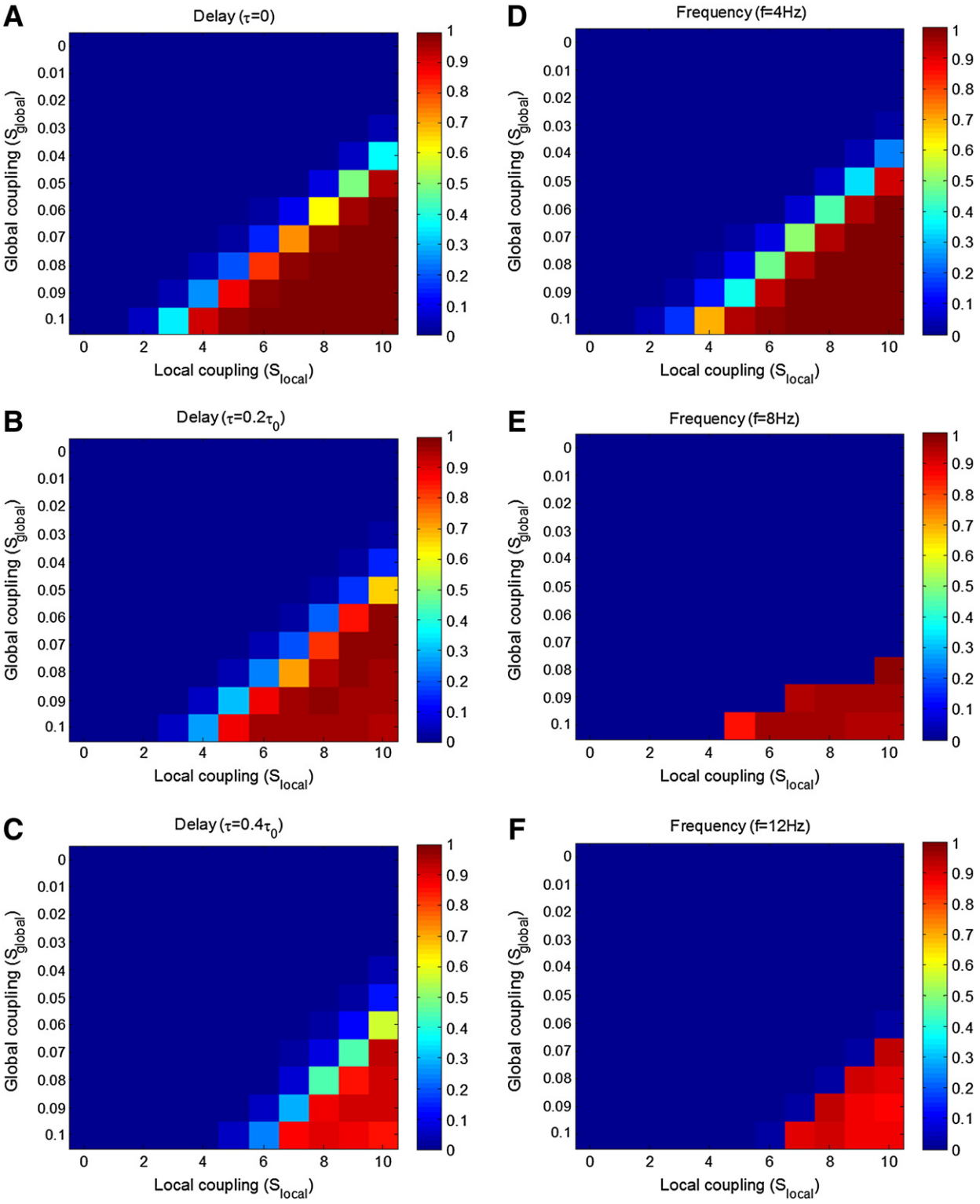

Fig. 9. Global synchronization in the parameter space of global and local coupling strength at different time delays and intrinsic frequencies. The X-axis represents the scaling factor of local coupling strength S_{local}, the Y-axis represents the scaling factor of global coupling strength S_{global}, and the color represents the amplitude of global order parameter. (A) Time delay $\tau = 0 (v = 0$ m/s) (intrinsic frequency $f = 4$ Hz). (B) Time delay $\tau = 0.2\tau_0 (v = 5$ m/s) (intrinsic frequency $f = 4$ Hz). (C) Time delay $\tau = 0.4\tau_0 (v = 2.5$ m/s) (intrinsic frequency $f = 4$ Hz). (D) Intrinsic frequency $f = 4$ Hz (time delay $\tau = 0.1\tau_0 (v = 10$ m/s)). (E) Intrinsic frequency $f = 8$ Hz (time delay $\tau = 0.1\tau_0 (v = 10$ m/s)). (F) Intrinsic frequency $f = 12$ Hz (time delay $\tau = 0.1\tau_0 (v = 10$ m/s)).

hubs identified (PFCORB and PFCCL) are highly ranked in the lists in Fig. 10. This means global synchronization is initialized from a few "hot spots" corresponding to brain areas with highest degree of centrality. In addition, as shown in the lists in Fig. 10, brain areas from frontal lobe are playing a dominant role in the initialization stage of the global synchronization.

Discussion

The choice of the model

As macroscopic models are very appropriate for describing epileptic processes occurring on large-scale, those models have been widely applied to explore the mechanisms underlying the EEG seizure patterns (Breakspear et al., 2006; Taylor and Baier, 2011; Wang et al., 2012; Wendling et al., 2002). In terms of the spike-wave discharges, an excellent example is the neural mass model proposed by the group of Lopes da Silva (Lopes da Silva et al., 2003). For a given set of parameters, the system has two simultaneous interictal and ictal

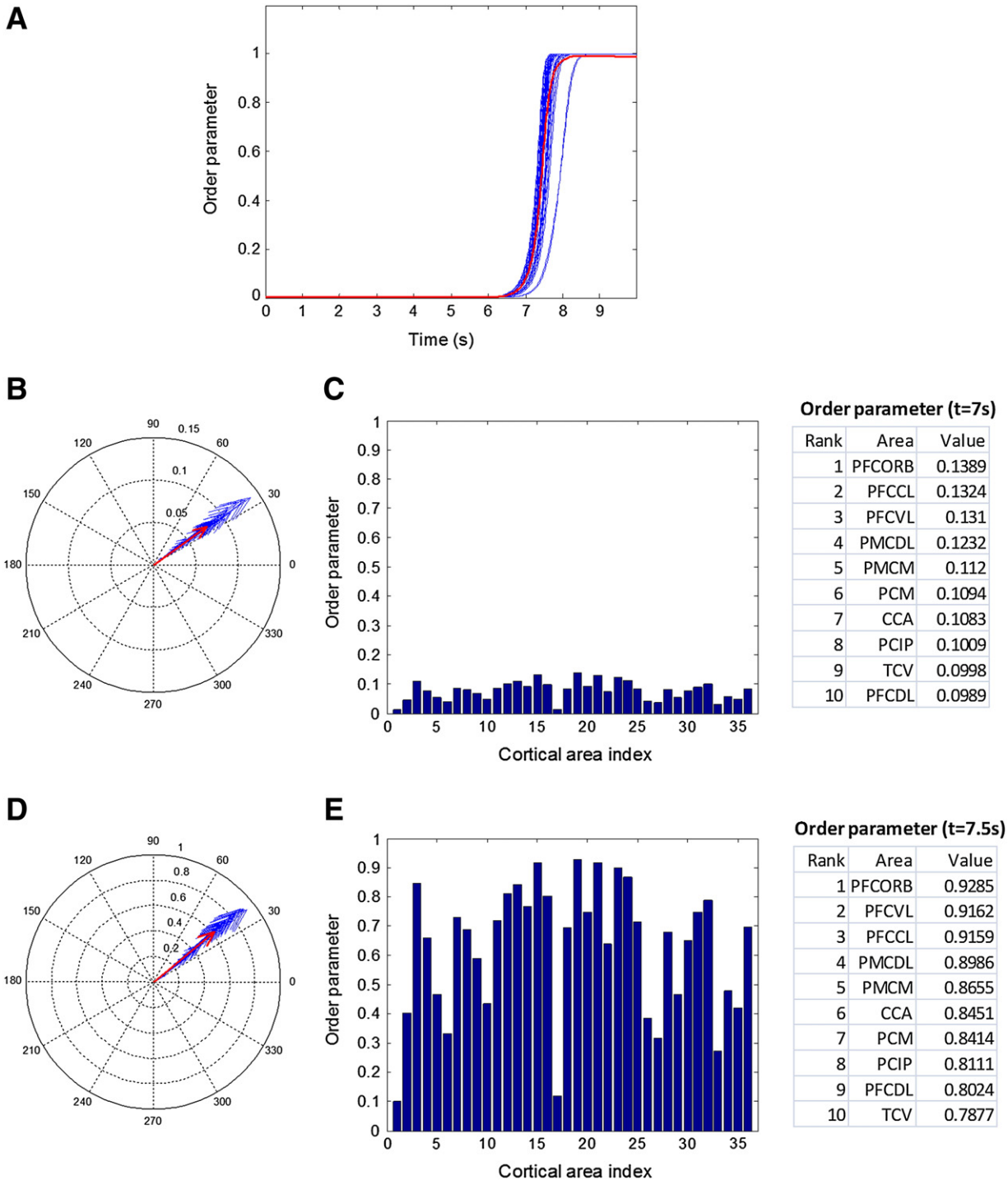

Fig. 10. The time courses of global and local synchronization. (A) The X-axis represents the time, and the Y-axis represents the amplitudes of order parameters. The blue lines represent the amplitudes of local order parameters of brain areas, and the red line represents the amplitude of the global order parameter. (B) The global (red) and local (blue) order parameters of brain areas in the polar coordinate system at $t=7$ s. (C) The Y-axis represents the amplitude of local order parameter and the X-axis represents the index of brain area at $t=7$ s. Top ten ranked brain areas for the amplitudes of local order parameters are listed in the table. (D) The global (red) and local (blue) order parameters of brain areas in the polar coordinate system at $t=7.5$ s. (E) The Y-axis represents the amplitude of local order parameter and the X-axis represents the index of brain area at $t=7.5$ s. Top ten ranked brain areas for the amplitudes of local order parameters are listed in the table.

attractors all the time, and to which attractor the trajectories converge, depends on the initial conditions and the system's parameters. Therefore, the model shows bistability with random external input as the bifurcation parameter, and transitions between normal and seizure states are caused by the variations in the external input.

In the past five years, neural field models have been successfully used to study resting-state brain networks (Cabral et al., 2011; Deco et al., 2009, 2011; Ghosh et al., 2008; Honey et al., 2007, 2009), where simulations are performed on biologically realistic connectivity of brain areas, and the neural dynamics at each brain area is modeled by a neural mass model (FitzHugh–Nagumo oscillator, Wilson–Cowan oscillator, etc). Similarly, those neural mass models can also be used to represent the dynamics of each area in the current study. Especially, the bistable model (Lopes da Silva et al., 2003) can be a good choice to describe the dynamics of each cortical area as a bistable switch characterized by the Hopf bifurcation. In this case, there are two stable states for each cortical area: a resting point representing the normal state of the brain and a limit cycle representing the seizure state. As the neural mass model actually describes the mean activity of neuronal population, the resting point statically represents a fully desynchronized state and the limit cycle represents a fully synchronized state of each cortical area.

However, in the current study, we take a different approach. Instead of modeling each cortical area as a neural mass model, we model each cortical area by a system of coupled oscillators described by Kuramoto models. Therefore, instead of representing the activity of cortical area by a fully synchronized state or a fully desynchronized state, we are capable of quantifying the degree of synchronization of each cortical area locally as well as the whole cortex globally. This offers a better observation of the evolution of synchronization in both time and space, and thus we can clearly see if some cortical areas are more synchronized than others, or some areas are getting synchronized earlier than others.

While suitable for describing the process of synchronization, we would like to point out that the current choice of model does have limitations in exploring the initialization of SWD. Especially, the current model does not have sufficient mechanisms to reproduce the prototypic waveform of SWD.

Relationship to cellular and synaptic mechanisms

Our study has suggested that the structural connectivity may play an important role in the generation of global synchronization and thus the abnormality of white matter may contribute to the emergence of SW epileptic seizures.

The suggested structural mechanism does not contradict the proposed cellular and synaptic mechanisms (de Curtis et al., 1998; Destexhe, 1998; Destexhe et al., 1996, 1998; Dichter and Ayala, 1987; Giaretta et al., 1987; Halliwell, 1986; Pollen, 1964; Schwindt et al., 1988; Timofeev and Steriade, 2004; Timofeev et al., 2004; Wong and Prince, 1978). It is possible that the combination of mechanisms from both perspectives leads to the initialization of SW epileptic seizures. From a dynamical system point of view, intuitively, there can be two regimes in a parameter space corresponding to whether or not a global synchronization can emerge. We refer to the regime where global synchronization emerges as a pathological regime and the other as a physiological regime. The divisions of the two regimes are largely determined by structural factors. For healthy individuals, the brain structure is configured such that their "operating points" are located deeply inside the physiological regime. On the other hand, for individuals suffering from SW epilepsy, while the "operating points" are still in the physiological regime most of the time, they are located so close to the boundary such that they can be temporarily driven across the boundary under parameter perturbation. The cellular and synaptic mechanisms may be responsive for such parameter perturbation. If the structure is configured in a way that global synchronization can easily unfold, a temporary imbalance between excitation and inhibition due to cellular and synaptic mechanisms may lead to SW epileptic seizures.

Note that, while intuitive, the above delineation of system can be too simplistic. Given the complexity of the system, it is necessary to explicitly study the role of node dynamics and network structure as an integrated whole. For example, in recent work (Gorochowski et al., 2011), a comprehensive formalism called Evolving Dynamical Network is introduced, and a new modeling framework is defined to incorporate network topology, dynamics, and evolution in an integrated way. This combination can be a potential candidate to explain the emergence of seizures because seizure generation typically involves the interplay of both node dynamics (cellular mechanisms) and network structure (synaptic connectivity).

Comparison with other experimentally inspired network studies

In fact, the abnormality of structural connectivity is often explored in a localized pathologic brain region, which is typically the focus of partial seizures. For example, in (Dyhrfjeld-Johnsen et al., 2007; Santhakumar et al., 2005), the abnormal structural changes (mossy fiber sprouting, mossy cell death, etc) in dentate gyrus are studied to explore the genesis of temporal lobe epilepsy. The current study differs from those works in the following aspects.

First, different types of epilepsies are being studied. While the current work studies the emergence of abnormal hypersynchronization (related to generalized spike-wave discharges) in the anatomical structural network of human brain, the work (Dyhrfjeld-Johnsen et al., 2007; Santhakumar et al., 2005) studies the genesis of temporal lobe epilepsy (a focal epilepsy). As a result, the abnormality of structural connectivity in (Dyhrfjeld-Johnsen et al., 2007; Santhakumar et al., 2005) was explored in the localized pathologic region (dentate gyrus, a part of hippocampal formation). Temporal lobe epilepsy is typically believed to be related to the structural change in the anatomy of dentate gyrus. In the surgically removed hippocampus from patients with temporal lobe epilepsy, there can be major changes in the anatomy of dentate gyrus including cell death, formation of new synaptic connections as axons sprout, etc.

Second, due to the differences in the object being studied, different computational models are being used as well. The current work is based on a macroscopic model, which is more appropriate for describing epileptic processes occurring on large-scale (such as the whole brain). The work (Dyhrfjeld-Johnsen et al., 2007; Santhakumar et al., 2005), on the other hand, is based on a detailed biophysical neuron network model of dentate gyrus.

White fiber abnormality

In this study, the role of brain structural connectivity in the emergence of global synchronization is examined by globally scaling the connectivity strength and fiber length matrices, which means the relative connectivity strength and fiber length between brain areas is assumed to be invariant. However, for patients with SW epileptic seizures, it is very possible that the relative connectivity strength and fiber length are varied. Recently, cross-sectional studies of children, adolescents and young adults with idiopathic generalized epilepsies (IGE) including childhood absence and juvenile myoclonic epilepsy have reported distributed patterns of abnormality predominantly affecting thalamus and frontal lobe (Betting et al., 2006a, 2006b, 2006c; Caplan et al., 2009a, 2009b; de Araujo et al., 2009; Kim et al., 2007; Pardoe et al., 2008; Pulsipher et al., 2009; Tae et al., 2006, 2008; Tosun et al., 2011). Collectively, these studies clearly indicate a neurodevelopmental contribution to anatomic abnormalities that have been observed in adults with these syndromes of epilepsy (Hermann et al., 2009). Along the same line, this may be able to explain the close relationship between absence epilepsy and

age. The fact that absence epilepsy can be outgrown might be related to the development of cortical connections, and there has been evidence suggesting that the development of cortical connections has a large influence on the coherence of brain activities. For example, a study (Thatcher et al., 2008) was conducted to explore human development of EEG coherence and phase differences over the period from infancy to 16 years of age. The results show that phase differences increase in the long inter-electrode distance as a function of age. The larger phase differences may imply that global synchronization becomes more difficult to happen as age increases. To fully shed light on this problem, more quantitative MRI studies examining patterns of brain development compared to healthy controls are needed, and it would be very interesting to carry out computational studies based on the brain connectivity of patients suffering from SW epilepsy.

The characteristic frequencies of global synchronization

In the past few years, existing computational studies have demonstrated the important role of the characteristic "small-world" structure of the underlying connectivity matrix between different brain areas in the spontaneous emergence of spatio-temporally structured network activities (Cabral et al., 2011; Deco et al., 2009, 2011; Ghosh et al., 2008; Honey et al., 2007, 2009). Especially, recent studies (Cabral et al., 2011; Deco et al., 2009) have revealed that the slow fluctuating and anti-correlated spatiotemporal patterns in resting state are linked to fluctuations in the neural activity and synchrony in the gamma range, and the most agreement occurs for a set of parameters (coupling, delay, noise, etc) where subsets of brain areas tend to synchronize in clusters while the network is not globally synchronized. In this computational study, we demonstrate another aspect of structural functional relationship at different time scales: while neural populations can exhibit oscillations in a wide range of frequency bands, global synchronization in the brain scale only occurs at low frequencies. We explain this by the interplay between time delays associated to the structural connectivity and intrinsic frequencies associated to neural populations. In this regard, we believe the low characteristic frequencies of SWD are partially owning to the underlying anatomical connectivity. More interestingly, our results agree with existing experimental observations: while long range synchronization at high frequencies (gamma rhythms) does exit in separate parts of the brain (Varela et al., 2001), the scale of such synchronization is quite limited compared with the generalized synchronization in SW epileptic seizures. Another thing worth mentioning is that, just like the resting state, global synchronization is another special case of the brain state. It would be much more difficult but worth investigating to explain the synchrony underlying normal brain functions in the presence of explicit tasks.

Frontal epileptic focus

By examining the interplay of local and global synchronization, our results not only demonstrate that the initialization of global synchronization has a clear anterior origin involving discrete areas of the frontal lobe (including dorsolateral part of superior frontal gyrus, supplementary motor area, middle frontal gyrus, etc), and but also indicate that the initialized areas of global synchronization("hot spots"), correspond to the nodes with highest degree of centrality ("structural hubs"). The observations of frontal focus are largely in agreement with experimental studies based on brain imaging techniques. For example, a study by Pavone showed that the origin of the spike-waves is cortical with maximal frontal lobe involvement (Pavone and Niedermeyer, 2000). Furthermore, a study by Holmes used high density EEG combined with an inverse problem algorithm to determine the location of the first SWD generators on an anatomical MRI template. Despite inter-individual variability in the precise location, the initial SWD had a clear anterior origin involving discrete focal regions of the frontal lobe (including dorsolateral, orbital and cingulum areas) (Holmes et al., 2004). More recently, a study by Amor (Amor et al., 2009) explored the spatiotemporal dynamics of interactions within and between widely distributed cortical sites using magnetoencephalographic recordings of absence seizures and revealed a multifocal fronto-central network, comprising the right prefrontal mesial, left orbitofrontal and left lateral postcentral areas of the cortex. While experimental observations of frontal epileptic focus do exist, there is a lack of understanding of the underlying mechanisms. To the best knowledge of the author, it is the first time that an explanation is given based on a computational study with the time-space structure of biologically realistic connectivity of 80 human cortical areas.

Note that, in the current study, all nodes are assumed to be identical and a "hot spot" simply means a node, which becomes synchronized earlier than others as a result of network structural connectivity. It does not mean the node in itself is abnormal, which drives the epileptic activity of the network. As a result, the current computational study cannot rule out the possibility that the node in itself is also abnormal. In fact, from a development point of view, due to some seizure induced changes, a normal node may also become abnormal if the network structure makes it always the starting point of seizures.

Acknowledgments

We thank Andrew Zalesky and Alex Fornito for the structural data for human brain connectivity.

References

Acebron, J.A., 2005. The Kuramoto model: a simple paradigm for synchronization phenomena. Rev. Mod. Phys. 77 (1), 137–185 (Jan).
Amor, F., Baillet, S., Navarro, V., Adam, C., Martinerie, J., Quyen, M.L.V., 2009. Cortical local and long-range synchronization interplay in human absence seizure initiation. NeuroImage 45, 950-862.
Arenas, A., Diaz-Guilera, A., Kurths, J., Moreno, Y., Zhou, C., 2008. Synchronization in complex networks. Phys. Rep. 469 (3), 93–153.
Benjamin, O., Fitzgerald, T.H.B., Ashwin, P., Tsaneva-Atanasova, K., Chowdhury, F., Richardson, M.P., Terry, J.R., 2012. A phenomenological model of seizure initiation suggests network structure may explain seizure frequency in idiopathic generalized epilepsy. J. Math. Neurosci. 2, 1 http://dx.doi.org/10.1186/2190–8567–2–1.
Betting, L.E., Mory, S.B., Li, L.M., Lopes-Cendes, I., Guerreiro, M.M., Guerreiro, C.A.M., Cendes, F., 2006a. MRI reveals structural abnormalities in patients with idiopathic generalized epilepsy. Neurology 67, 848–852.
Betting, L.E., Mory, S.B., Li, L.M., Lopes-Cendes, I., Guerreiro, M.M., Guerreiro, C.A.M., Cendes, F., 2006b. MRI volumetry shows increased anterior thalamic volumes in patients with absence seizures. Epilepsy Behav. 8, 575–580.
Betting, L.E., Mory, S.B., Li, L.M., Lopes-Cendes, I., Guerreiro, M.M., Guerreiro, C.A.M., Cendes, F., 2006c. Voxel-based morphometry in patients with idiopathic generalized epilepsies. NeuroImage 32, 498–502.
Breakspear, M., Roberts, J.A., Terry, J.R., Rodrigues, S., Mahant, N., Robinson, P.A., 2006. A unifying explanation of primary generalized seizures through nonlinear brain modeling and bifurcation analysis. Cereb. Cortex 16, 1296–1313.
Breakspear, M., Heitmann, S., Daffertshofer, A., 2010. Generative models of cortical oscillations: neurobiological implications of the Kuramoto model. Front. Hum. Neurosci. 4, 190 http://dx.doi.org/10.3389/fnhum.2010.00190 (Nov).
Cabral, J., Hugues, E., Sporns, O., Deco, G., 2011. Role of local network oscillations in resting-state functional connectivity. Front. Hum. Neurosci. 1 (57), 130–139 (Jul).
Caplan, R., Levitt, J., Siddarth, P., Wu, K.N., Gurbani, S., Sankar, R., Shields, W.D., 2009a. Frontal and temporal volumes in childhood absence epilepsy. Epilepsia 50 (11), 2466–2472.
Caplan, R., Levitts, J., Siddarth, P., Wu, K.N., Gurbani, S., 2009b. Language and frontotemporal volumes in pediatric epilepsy. Epilepsy Behav. 17 (3), 402–407.
de Araujo, G.M., Jackowski, A.P., Lin, K., Guaranha, M.S.B., Guilhoto, L.M.F.F., da Silva, H.H., Caboclo, L.O.S.F., Garrete, H., Bressan, R.A., Yacubian, E.M.T., 2009. Personality traits related to juvenile myoclonic epilepsy: MRI reveals prefrontal abnormalities through a voxel-based morphometry study. Epilepsy Behav. 15 (2), 202–207.
de Curtis, M., Radici, C., Forti, M., 1998. Cellular mechanisms underlying spontaenous intericatal spikes in an acute model of focal cortical epileptogenesis. Neuroscience 88, 107–117.
Deco, G., Jirsa, V.K., McIntosh, A.R., Sporns, O., Kotter, R., 2009. Key role of coupling, delay, and noise in resting brain fluctuations. Proc. Natl. Acad. Sci. 106 (25), 10302–10307 (June).
Deco, G., Jirsa, V.K., McIntosh, A.R., 2011. Emerging concepts for the dynamical organization of resting-state activity in the brain. Nat. Rev. Neurosci. 12, 43–56 (Jan.).
Destexhe, A., 1998. Spike-and-wave oscillations based on the properties of GABA(B) receptors. J. Neurosci. 18, 9099–9111.

Destexhe, A., Bal, T., McCormick, D.A., Sejnowski, T.J., 1996. Ionic mechanisms underlying synchronizing oscillations and propagating waves in a model of ferret thalamic slices. J. Neurophysiol. 76, 2049–2070.
Destexhe, A., Contreras, D., Steriade, M., 1998. Mechanisms underlying the synchronizing action of corticothalamic feedback through inhibition of thalamic relay cells. J. Neurophysiol. 79, 999–1016.
Dichter, M.A., Ayala, G.F., 1987. Cellular mechanisms of epilepsy: a status report. Science 237, 157–164.
Dyhrfjeld-Johnsen, J., Santhakumar, V., Morgan, R.J., Huerta, R., Tsimring, L., Soltesz, I., 2007. Topological determinants of epileptogenesis in large-scale structural and functional models of the dentate gyrus derived from experimental data. J. Neurophysiol. 97, 1566–1587.
Ghosh, A., Rho, Y., McIntosh, A.R., Kotter, R., Jirsa, V.K., 2008. Noise during rest enables the exploration of the brain's dynamic repertoire. PLoS Comput. Biol. 4 (10), e1000196 http://dx.doi.org/10.1371/journal.pcbi.1000196 (Oct.).
Giaretta, D., Avoli, M., Gloor, P., 1987. Intracellular recordings in pericruciate neurons during spike and wave discharges of feline generalized penicillin epilepsy. Brain Res. 405, 68–79.
Goodfellow, M., Schindler, K., Baier, G., 2011. Intermittent spike-wave dynamics in a heterogeneous, spatially extended neural mass model. NeuroImage 55, 920–932.
Gorochowski, T.E., Bernardo, M.D., Grierson, C.S., 2011. Evolving dynamical networks: a formalism for describing complex systems. Complexity 17 (3), 18–25.
Halliwell, J.V., 1986. M-current in human neocortical neurones. Neurosci. Lett. 67 (1), 1–6.
Hermann, B.P., Jones, J.J., Jones, J.E., Seidenberg, M., 2009. The emerging architecture of neuropsychological impairment in epilepsy. Neurol. Clin. 27 (4), 881–907.
Holmes, M.D., Brown, M., Tucker, D.M., 2004. Are generalized seizures truly generalized? Evidence of localized mesial frontal and frontopolar discharges in absence. Epilepsia 45 (12), 1568–1579.
Honey, C.J., Kotter, R., Breakspear, M., Sporns, O., 2007. Network structure of cerebral cortex shapes functional connectivity on multiple time scales. Proc. Natl. Acad. Sci. 104 (24), 10240–10245 (Jun.).
Honey, C.J., Sporns, O., Cammoun, L., Gigandet, X., Thiran, J.P., Meuli, R., Hagmann, P., 2009. Predicting human resting-state functional connectivity from structural connectivity. Proc. Natl. Acad. Sci. 106 (6), 2035–2040 (Feb.).
Kim, J.H., Lee, J.K., Koh, S.B., Lee, S.A., Lee, J.M., Kim, S.I., Kang, J.K., 2007. Regional grey matter abnormalities in juvenile myoclonic epilepsy: a voxel-based morphometry study. NeuroImage 37 (4), 1132–1137.
Kitzbichler, M.G., Smith, M.L., Christensen, S.R., Bullmore, E., 2009. Broadband criticality of human brain network synchronization. PLoS Comput. Biol. 5 (3), e1000314 http://dx.doi.org/10.1371/journal.pcbi.1000314.
Kotter, R., 2004. Online retrieval. processing, and visualization of primate connectivity data from the CoCoMac database. Neuroinformatics 2, 127–144.
Kuramoto, Y., 1984. Chemical Oscillations, Waves and Turbulence. Springer, New York.
Lopes da Silva, F.H., Blanes, W., Kalitzin, S.N., parra, J., Suffczynski, P., Velis, D.N., 2003. Dynamical diseases of brain systems: different routs to epileptic seizures. IEEE Trans. Biomed. Eng. 50, 540–548.
Lytton, W.W., 2008. Computer modelling of epilepsy. Nat. Rev. Neurosci. 9, 626–637 (Aug.).
Pardoe, H., Pell, G.S., Abbott, D.F., Berg, A.T., Jackson, G.D., 2008. Multi-site voxel-based morphometry: methods and a feasibility demonstration with childhood absence epilepsy. NeuroImage 42 (2), 611–616.
Pavone, A., Niedermeyer, E., 2000. Absence seizures and the frontal lobe. Clin. Electroencephalogr. 31 (3), 153–156 (Jul).
Pollen, D.A., 1964. Intracellular studies of cortical neurons during thalamic induced wave and spike. Electroencephalogr. Clin. Neurophysiol. 17, 398–404.
Pulsipher, D.T., Seidenberg, M., Guidotti, L., Tuchscherer, V.N., Morton, J., Sheth, R.D., Hermann, B., 2009. Thalamofrontal circuitry and executive dysfunction in recent-onset juvenile myoclonic epilepsy. Epilepsia 50 (5), 1210–1219.
Rubinov, M., Sporns, O., 2010. Complex network measures of brain connectivity: uses and interpretations. NeuroImage 52, 1059–1069.
Santhakumar, V., Aradi, I., Soltesz, I., 2005. Role of mossy fiber sprouting and mossy cell loss in hyperexcitability: a network model of the dentate gyrus incorporating cell types and axonal topography. J. Neurophysiol. 93, 437–453.
Schwindt, P.C., Spain, W.J., Foehring, R.C., Stafstrom, C.E., Chubb, M.C., Crill, W.E., 1988. Multiple potassium conductances and their functions in neurons from cat sensorimotor cortex in vitro. J. Neurophysiol. 59, 424–449.
Tae, W.S., Hong, S.B., Joo, E.Y., Han, S.J., Cho, J.W., Seo, D.W., Lee, J.M., Kim, I.J., Byun, H.S., Kim, S.I., 2006. Structural brain abnormalities in juvenile myoclonic epilepsy patients: volumetry and voxel-based morphometry. Korean J. Radiol. 7 (3), 162–172.
Tae, W.S., Kim, S.H., Joo, E.Y., Han, S.J., Kim, I.Y., Kim, S.I., Lee, J.M., Hong, S.B., 2008. Cortical thickness abnormality in juvenile myoclonic epilepsy. J. Neurol. 255 (4), 561–566.
Taylor, P.N., Baier, G., 2011. A spatially extended model for macroscopic spike-wave discharges. J. Comput. Neurosci. 31, 679–684.
Terry, J.R., Benjamin, Q., Richardson, M.P., 2012. Seizure generation: the role of nodes and networks. Epilepsia http://dx.doi.org/10.1111/j.1528-1167.2012.03560.x.
Thatcher, R.W., North, D.M., Biver, C.J., 2008. Development of cortical connections as measured by EEG coherence and phase delays. Hum. Brain Mapp. 29, 1400–1415.
Timofeev, I., Steriade, M., 2004. Neocortical seizures: initiation, development and cessation. Neuroscience 123, 299–336.
Timofeev, I., Grenier, F., Steriade, M., 2004. Contribution of intrinsic neuronal factors in the generation of cortically driven electrographic seizures. J. Neurophysiol. 92, 1138–1143.
Tosun, D., Dabbs, K., Caplan, R., Siddarth, P., Toga, A., Seidenberg, M., Hermann, B., 2011. Deformation-based morphometry of prospective neurodevelopmental changes in new onset paediatric epilepsy. Brain 134 (4), 1003–1014 (April).
Tzourio-Mazoyer, N., Landeau, B., Papathanassiou, D., Crivello, F., Etard, O., Delcroix, N., Mazoyer, B., Joliot, M., 2002. Automated anatomical labeling of activations in SPM using a macroscopic anatomical parcellation of the MNI MRI single-subject brain. NeuroImage 15 (1), 273–289 (Jan).
Uhlhaas, P.J., Singer, W., 2006. Neural synchrony in brain disorders: relevance for cognitive dysfunctions and pathophysiology. Neuron 52, 155–168.
Varela, F., Lachaux, J., Rodriguez, E., Martinerie, J., 2001. The brainweb: phase synchronization and large-scale integration. Nat. Rev. Neurosci. 2 (4), 229–239.
Wang, Y., Goodfellow, M., Taylor, P.N., Baier, G., 2012. Phase space approach for modeling of epileptic dynamics. Phys. Rev. E 85 (6) http://dx.doi.org/10.1103/PhysRevE.85.061918.
Wendling, F., Bartolomei, F., Bellanger, J.J., Chauvel, P., 2002. Epileptic fast activity can be explained by a model of impaired GABAergic dendritic inhibition. Eur. J. Neurosci. 15 (9), 1499–1508.
Wong, R.K., Prince, D.A., 1978. Participation of calcium spikes during intrinsic burst firing in hippocampal neurons. Brain Res. 159 (2), 385–390.
Yan, B., Li, P., 2011. An integrative view of mechanisms underlying generalized spike-and-wave epileptic seizures and its implication on optimal therapeutic treatments. PLoS One 6 (7), e22440 http://dx.doi.org/10.1371/journal.pone.0022440 (July).
Zalesky, A., Fornito, A., 2009. A DTI-derived measure of cortico-cortical connectivity. IEEE Trans. Med. Imaging 28 (7), 1023–1036 (Jul.).